Cold Side Thermal Energy Storage System For Improved Operation of Air Cooled Power Plants

by

Daniel David Williams

Submitted to the Department of Mechanical Engineering
in partial fulfillment of the requirements for the degree of

Master of Science in Mechanical Engineering

at the

MASSACHUSETTS INSTITUTE OF TECHNOLOGY

September 2012

Author .....
Department of Mechanical Engineering
August 20, 2012

Certified by .....
Alexander Mitsos
Rockwell International Assistant Professor
Thesis Supervisor

Accepted by .....
David E. Hardt
Ralph E. and Eloise F. Cross Professor of Mechanical Engineering
Chairman, Department Committee on Graduate Theses

Cold Side Thermal Energy Storage System For Improved Operation of Air Cooled Power Plants

by

Daniel David Williams

Submitted to the Department of Mechanical Engineering
on August 20, 2012, in partial fulfillment of the
requirements for the degree of
Master of Science in Mechanical Engineering

Abstract

Air cooled power plants experience significant performance fluctuations as plant cooling capacity reduces due to higher daytime temperature than nighttime temperature. The purpose of this thesis is to simulate the detailed operation of a cold side thermal energy storage system in order to evaluate its potential. An organic Rankine cycle geothermal power station is used as an example application. Detailed sizing and operation considerations are discussed. Several representative case studies compare the performance of candidate configurations. Operation of the selected configuration is then simulated for a full year and a proposed integration of the system with existing plant hardware is laid out. A correlation between weather trends and production is outlined. Finally an economic cost/benefit analysis performed to determine the payback period for implementing the proposed system.

The cold side TES system is shown to shift substantial power generation capability from nighttime to daytime when electrical demand is highest, especially during hot summer months. For example, daily energy production is shown to increase by up to 18% under particularly favorable conditions. This redistribution of the power generation curve is accomplished with less than a 5% reduction in overall annual energy production in Mega-Watt hours. The system is shown to be more effective at shifting power generation capacity during warmer months than cooler months. The reduced day to night temperature fluctuation during cooler months results in a reduced thermal storage benefit under similar parasitic loads.

The economic benefits of this system are dependent upon the on-peak vs off-peak electricity prices. Economic analysis using 2011 transient price data from the U.S. Midwest Region results in a small increase in annual income. The increased income from the proposed cold side TES system is found to be insufficient to outweigh the required capital investment at current electricity prices.

Thesis Supervisor: Alexander Mitsos
Title: Rockwell International Assistant Professor

Acknowledgments

First and foremost, I am thankful to my advisor, Dr. Alexander Mitsos, whose guidance and support enabled me to develop this thesis from a concept to a completed work. His attention to detail and expertise were essential to ensuring a thorough study and have greatly contributed to my own understanding of the subject matter. Equally important was Dr. Mitsos sincerity and encouraging demeanor in dealing with the challenges associated with splitting my time between my academic work and full time employment responsibilities.

I am grateful for the contributions of Dr. Hadi Ghasemi who was instrumental in solidifying my understanding of the operation of the Salt Wells geothermal facility. His modeling and data matching work regarding the existing plant machinery formed the foundation from which my proposed system model could be built.

I would like to acknowledge the technical contribution of Enrique Lizarraga who in the course of his thesis work developed a technique by which a modified 2D plug flow simulation may be used to model turbulent pipe flow heat exchange COMSOL Multiphysics®. This technique was responsible for a dramatic reduction in computing time versus employing a turbulent flow solver while still allowing precise control over the heat transfer characteristics of the system.

I would like to thank Nick Macini who developed the initial concept of a coldside thermal energy storage system. His preliminary hand calculations were the motivation for further study that eventually yielded this thesis.

I would like to thank Gina Zak for her constant patient assistance in teaching me several of the software applications required to prepare this work. I am particularly thankful for Gina's help while formatting and compiling this document.

I would also like to thank the General Electric Company for funding my graduate work and for facilitating a leave of absence to complete my thesis. The company's commitment to education is apparent in all levels of corporate leadership. I would like to thank Ken Gould, coordinator of the GE Lynn Advanced Course in Engineering, in particular for his steadfast encouragement and mentorship.

Contents

List of Figures

List of Tables

Nomenclature

Latin Letters

A	Area	m^2
Bi	Biot Number	
C	Heat Capacity of a Solid	$\frac{J}{kg \cdot K}$
D	Diameter	m
h	Specific Enthalpy	$\frac{J}{kg}$
f	Darcy Friction Factor	
$\dot{Q}$	Heat rejection rate	W
c	Convective heat transfer coefficient	$\frac{W}{m^2 K}$
k	Thermal Conductivity	$\frac{W}{m \cdot K}$
L	Length	m
$\dot{m}$	Mass Flow Rate	$\frac{kg}{s}$
M	Mass	kg
n	Number of Pipes	
Nu	Nusselt Number	
T	Temperature	K
thk	Thickness	m
p	Pressure	$\frac{N}{m^2}$
V	Volume	m^3
v	Velocity	$\frac{m}{s}$
$\dot{W}$	Power	W
x	Axial coordinate	m

Abbreviatons

ACC	Air Cooled Condenser	
ACHX	Air Cooled Heat Exchanger	
CC	Capital Cost to construct system	\$
MP	Material Price	
OCC	Oil Cooled Condenser	
TES	Thermal Energy Storage	

Greek Letters

Δ	Change	
ρ	Density	$\frac{\text{kg}}{\text{m}^3}$
μ	Dynamic Viscosity	$\text{Pa} \cdot \text{s}$

Subscripts

axial	Along the axis of the pipe
c	Characteristic
concrete	Concrete material
condensing	Phase change from vapor to liquid
cross-section	Cross section perpendicular to pipe axis
D	Calculated using the diameter
fg	Pertaining to complete phase change
conv	Temperature drop calculated as a function of the fluid to wall convective heat transfer coefficient only
h	Hydraulic
isobutane	Pertaining to isobutane

1	Beginning of TES heating phase
o	Outer
oil	Liquid heat exchange oil
oil-pipe	Pertaining to the oil flowing through a single pipe in the pipe array
pipe	Pertaining to a single TES pipe
pipe wall	Pertaining to the metallic pipe wall
pipes	Pertaining to all of the pipes in the pipe array
solid	Solid thermal storage medium
2	End of TES heating phase
oil-total	Pertaining to the oil flowing through the entire pipe array
TES Pump	Pertaining to the TES oil pump
U	Temperature drop calculated as a function of the fluid to wall convective heat transfer coefficient and conductive resistance of the solid thermal storage medium

Chapter 1

Introduction

1.1 Power Plant Heat Rejection Methods

While the quality of a power plant's heat source influences working fluid selection, cycle configuration and the system efficiency, the method of heat rejection also has a notable effect on the system performance. Even at Carnot efficiency, the heat rejection requirements of a geothermal power plant can be an order of magnitude greater than the usable power produced. Often the hot source is not a reservoir as assumed in the Carnot efficiency but rather a hot stream, e.g., the flue gases in coal plants or the brine in binary geothermal plants. In that case the theoretical limit is given by the so-called modified Carnot efficiency Figure 1-1 shows the modified Carnot efficiency versus heat source temperature for heat rejection temperatures associated with arid climate daytime and nighttime operation. The physical interpretation of this figure for Rankine cycles is that heat rejection at lower temperature allows for lower condenser operating pressure. This increases the pressure drop across the power turbine and thus the power produced.

Plants located with ready access to large bodies of water can utilize a liquid cooled condenser to employ a river or ocean as a cold sink. This method requires very little parasitic load for cooling water pumping and the footprint of heat rejection apparatus is limited to a liquid-liquid heat exchanger. The temperature of a suitably large body of water can change with the seasons, but the period of such changes is on the order

of months.

Some plant locations are remote to large bodies of water, but still have a reasonably inexpensive water supply. Given low humidity ambient conditions, such facilities can use evaporative cooling techniques to condense to temperatures near the ambient wet bulb temperature. This temperature fluctuates with the ambient temperature and relative humidity. Evaporative cooling systems require either a higher parasitic load to drive fans and/or increased capital and footprint to erect natural draft towers.

A third cooling scenario arises in arid climates where water is expensive, if not unavailable, for industrial purposes. In this case, heat rejection is accomplished by an air cooled condenser. An air cooled condenser (ACC) utilizes fans to create a draft over finned heat exchange tubes. These units tend to have a substantial footprint and can require a significant parasitic load to drive the fans. For the example system the parasitic load from the ACC fans can account for a significant portion of the gross turbine output, depending on ambient conditions. The condenser operating pressure is also highly dependent on ambient dry bulb temperature, which fluctuates significantly from night to day.

1.2 Geothermal Power

Geothermal power is a method of electricity generation that utilizes geothermal fluid heated by hot subterranean rock as a heat source. The rocks in the earth's crust are heated by a combination of residual heat from the formation of the planet and radioactive decay of several isotopes trapped in the rock. Most of the earth's surface is covered by a relatively thick layer of uninterrupted crust that serves to insulate the surface from the extreme magma temperatures found at depth. However, in some places geological formations such as fault lines and fractures in the earth's crust allow fluids such as magma or aquifer water to more efficiently carry the geothermal heat closer to the surface. In such locations a usable heat source is accessible at a reasonable drilling depth. [4]

Geothermal heat can be utilized in several ways. Lower temperature geothermal

formations, such as the example plant discussed here, are unable to directly utilize geothermal steam. Therefore, they require more complex binary cycles such as an Organic Rankine cycle or the ammonia based Kalina Cycle. Hot brine is used to vaporize a low boiling point working fluid via an evaporator. Binary cycle plants seek to make up some of the efficiency losses due to low temperature heat sources by employing recuperators and more complex flowsheets. [4]

1.3 Motivation

This thesis focuses specifically on the challenge of improving cold sink behavior of a power station in an arid climate where evaporative cooling is impractical. Many of the world's identified geothermal resources are located in hot and dry regions such as the American southwest and their development is dependent on some form of air cooled heat rejection system.

Dry air cooled condensers are susceptible to significant performance degradation as ambient temperatures increase during the day. Because geothermal power relies on a relatively low temperature heat source the overall cycle efficiency is more sensitive to fluctuations in the cold sink temperature than other power production technologies.

Much of this capability is recovered as ambient temperatures fall during the night, but (like many renewable technologies) these performance transients do not correspond with fluctuations in typical demand profiles. See Figure 1-3 depicting several U.S. demand curves. Also see Figure 1-4 depicting ambient temperature and the example plant output versus time of day. Notice that as demand is rising up to a peak in early afternoon, the output of the plant is falling because the ACC's cannot reject sufficient heat to the hot ambient air. It is desirable to develop a system by which the cooler night time temperatures can be used to improve plant performance during the warmer daytime hours when demand (and therefore electricity price) is elevated.

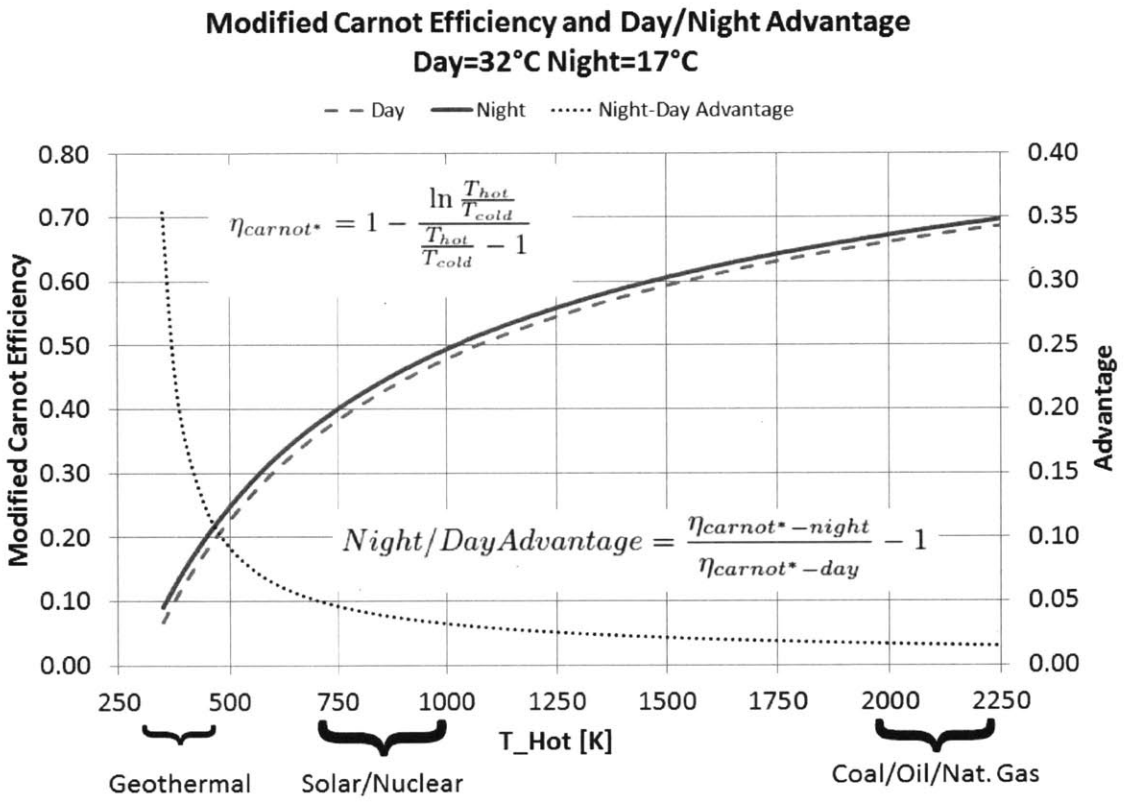

Figure 1-1: Modified Carnot Efficiency and Day/Night Advantage

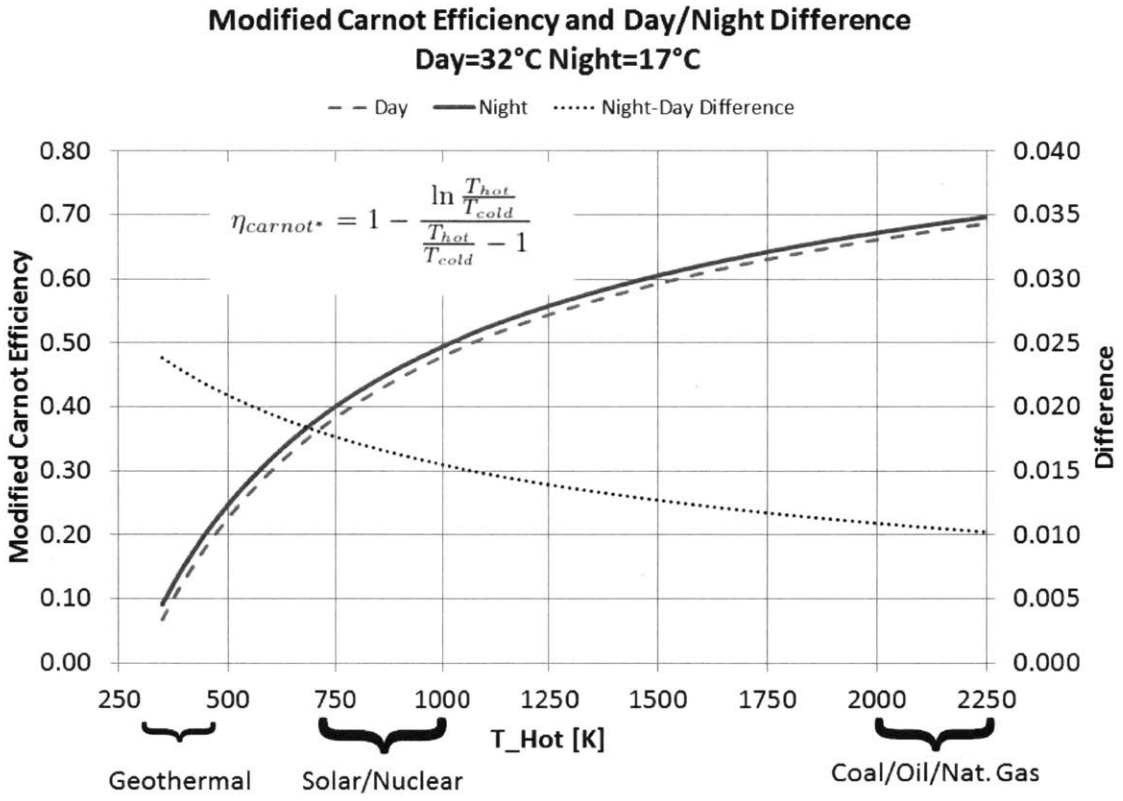

Figure 1-2: Modified Carnot Efficiency and Day/Night Difference

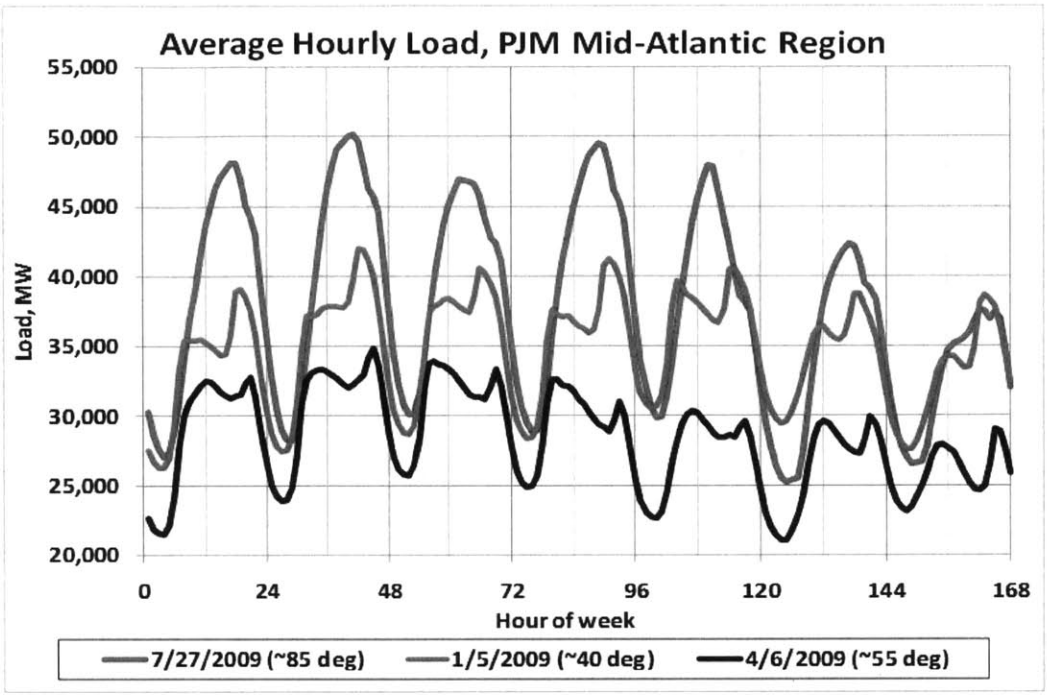

Figure 1-3: Typical Load Curves
[9]

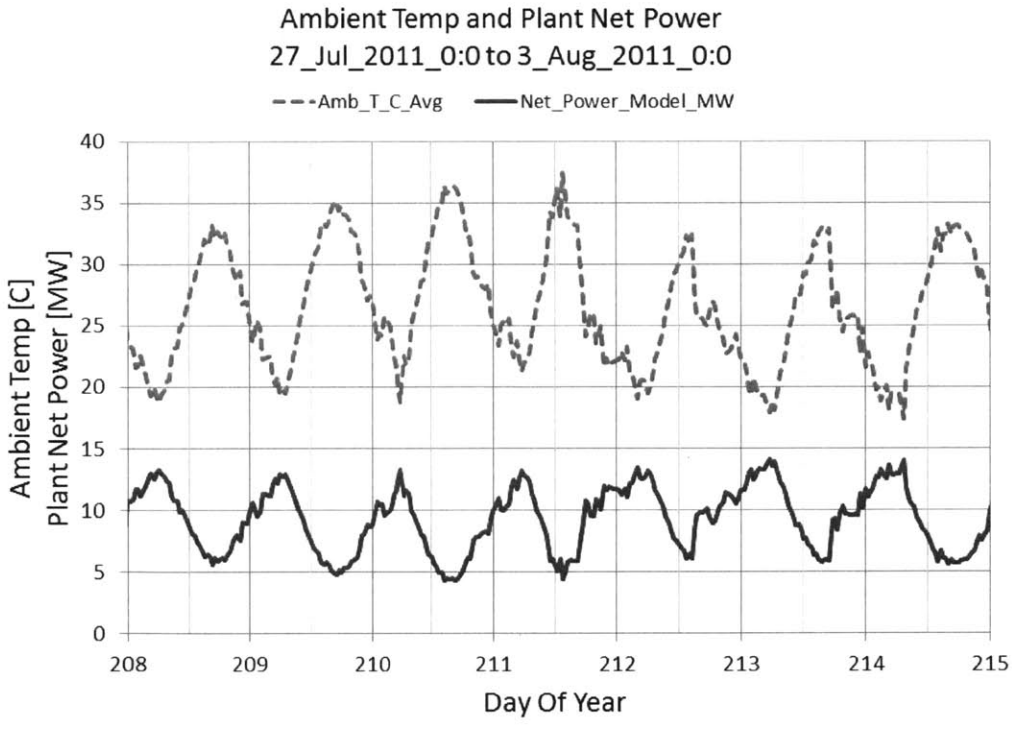

Figure 1-4: Ambient Temperature and Net Plant Output [5]

1.4 Objectives

The primary purpose of this thesis is to assess the potential benefits of a cold side thermal energy storage system. While a cold side thermal energy storage system is applicable to many types of power plants this thesis intends to demonstrate the value of applying one to a geothermal power plant. Geothermal power plants are uniquely dependent on geological formations that sometimes necessitate their construction in the hot, arid climates where heat rejection is difficult.

The secondary goal of this thesis is to perform a rough economic analysis, comparing the financial benefits of implementing the proposed system to the capital costs required.

1.5 Model of Existing Plant

A cycle model of an operational geothermal power plant is employed to model the plant performance with and without a cold side TES system. The 20 MW Salt Wells facility is operated by the Italian electric utility Ente Nazionale per l'Energia eLettrica (ENEL). Salt Wells is located on a remote location in Fallon Nevada USA. The plant employs isobutane working fluid in an organic Rankine cycle and depends solely on air cooled condensers for heat rejection to the atmosphere.

Ghasemi and Mitsos [5] have developed a comprehensive pseudo steady-state model of the plants operation based on equipment specifications and operating data provided by ENEL. Their validated model of current operation is used as the baseline for this study.

For the purposes of this study only certain operating parameters and the detailed specifications of the ACCs are considered. The geothermal brine flow rate and incoming temperature are assumed to be constant. Therefore, the gross turbine power output is dependent on the pressure that can be maintained in the condenser. Figure 1-5 shows the effective flowsheet operating mode for the existing system as it pertains to this study. For the purposes of this study, this is called operating mode 1. The

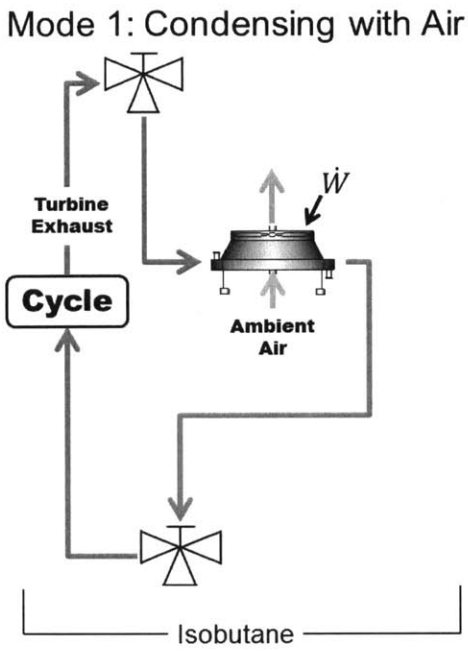

Figure 1-5: Existing System Operating Mode

TES system adds two additional modes that are described in detail in subsequent sections.

Performance curves represent the effective behavior of the complex cycle as a function of ambient temperature. Figure 1-6 relates turbine gross power to condenser pressure and Figure 1-7 shows the relationship between condenser pressure and ambient temperature for the existing 126 fan ACC. The flat part of the pressure vs ambient temperature curve is due to turbine operating limitations that require a minimum condenser pressure of 300 kPa. These curves combine to yield the relationship between turbine gross power and ambient temperature of Figure 1-8.

One third of the ACC fans operate at a constant speed and the other two-thirds are adjustable. This allows for reduced parasitic load when the minimum condenser pressure is achieved during cold weather. Figure 1-9 shows the power required to run the 126 fan ACC unit as a function of ambient temperature.

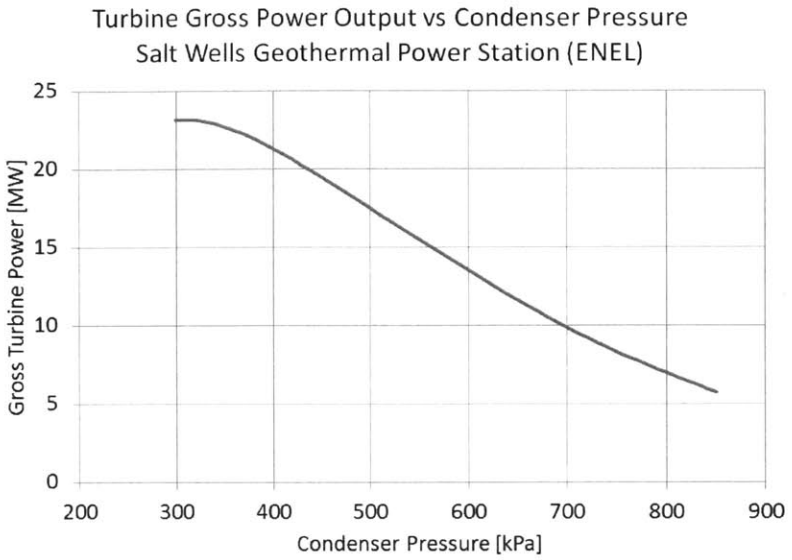

Figure 1-6: Turbine Gross Power Output vs Condenser Pressure for Salt Wells Plant [5]

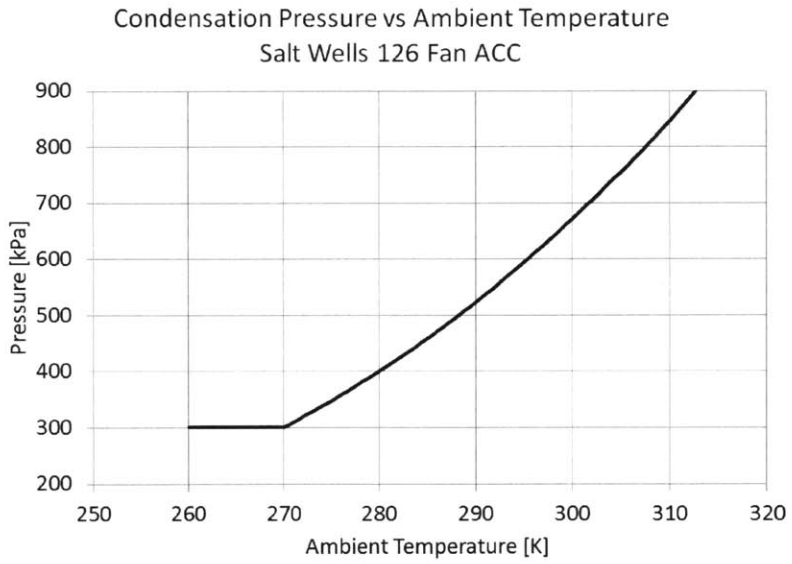

Figure 1-7: ACC Condenser Pressure vs Ambient Temperature for Existing Salt Wells 126 Fan ACC

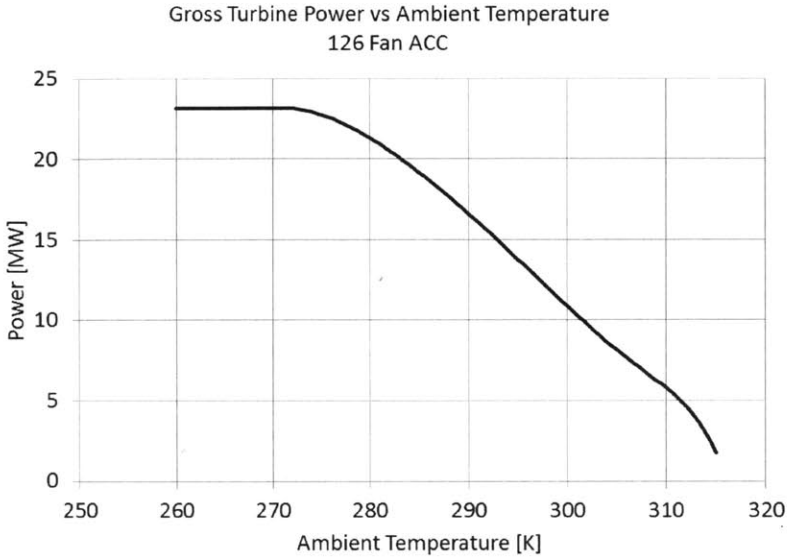

Figure 1-8: Turbine Gross Power Output vs Ambient Temperature for Existing Salt Wells Plant

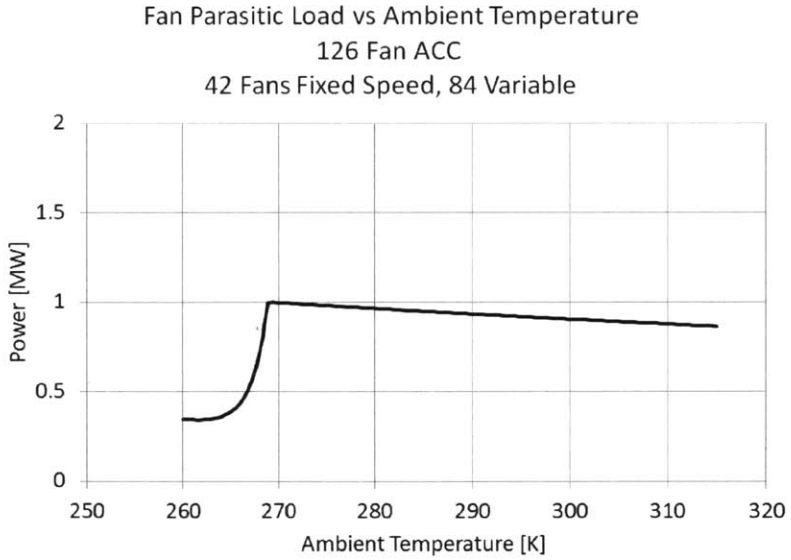

Figure 1-9: ACC Fan Parasitic Load vs Ambient Temperature

1.6 Proposed System

The proposed cold side thermal energy storage (TES) system uses a large concrete block as the thermal storage medium. Iron pipes pass through the concrete block to carry heat exchanger oil. During periods of cool ambient temperature the geothermal plant operates as usual, employing ACCs to condense the Isobutane working fluid. Meanwhile, the TES system is cooled by circulating the heat exchanger oil through an air cooled heat exchanger (ACHX) and the concrete block, thus cooling it. This is Mode 2. At a given time of day, the system switches from cooling the TES to using the TES as the cold sink (Mode 3). This is accomplished by routing the Isobutane working fluid through an oil cooled condenser (OCC) which is cooled by the TES heat exchange oil. As this operation proceeds, the TES is gradually warmed until the system is once again switched into cooling mode (Mode 2). The system is also capable of operating in mode 1, ACCs used to condense the working fluid without the TES or ACHX active, under certain circumstances.

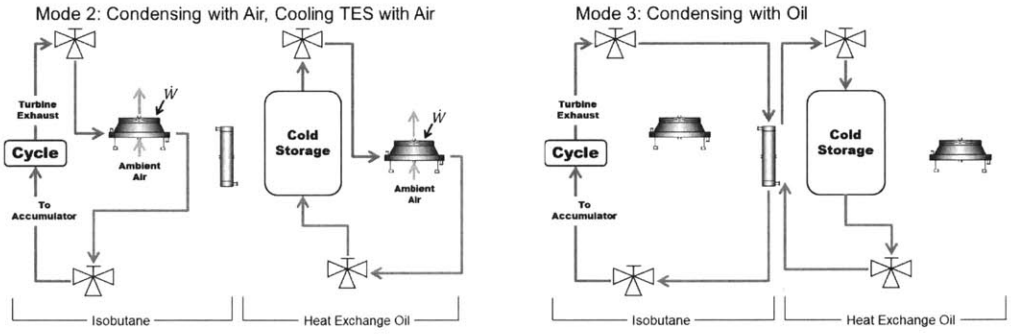

(a) Coldside TES Cooling

(b) Coldside TES Heating

Figure 1-10: Proposed System Operating Modes

Chapter 2

Procedure

2.1 TES Sizing

The sizing of the Artificial Cold Sink system has two main considerations. The first is ensuring sufficient thermal mass to store the required heating load for the desired amount of time. The second consideration is designing the pipe geometry, concrete geometry and flow rates such that the required heat exchange is accomplished with a reasonable temperature differential under design conditions. The following thermal storage capacity equation relates the heat rejection required during TES enhanced condensing with the thermal capacity of the TES block and the anticipated temperature change of the TES block.

$$\text{Capacity} = \dot{Q}_{\text{condensing}} \cdot t_{\text{condensing}} = V_{\text{solid}} \cdot \rho_{\text{solid}} \cdot C_{\text{solid}} \cdot (T_2 - T_1)$$

The first step in assigning a design capacity is determining how long the storage medium is utilized as a cold sink between cooling sessions. For instance, the system could be designed to store cold all winter and use it all summer. Or the system could be sized to store cold overnight and expend its stores the following day. The daily and seasonal transient behavior of ambient temperature must be understood in order to make this assessment. Figure 2-1 shows the minimum and maximum daily temperatures for a full year from November 2010 to November 2011. Figures 2-2

and 2-3 show ambient temperature fluctuations at a 30 minute resolution and daily minimum and maximum temperatures for January and July 2011 respectively.

Examination of the daily minimum and maximum temperatures for one year show clear seasonal trends. Both minimum and maximum temperatures trend towards their peak in the summer months and tend to be lowest in the winter months. The separation between minimum and maximum daily temperature is most predictably large in the summer months and to a lesser extent in the autumn months. However, during the winter months the distribution becomes more erratic. Some days have particularly high lows that could exceed the high of a few days later.

These studies show that ambient temperature drops very reliably from day to night during the warmest months. This is also when performance is most severely impacted by high daytime temperatures. A storage capacity for one day of usage is chosen in order to successfully capitalize on the predictable temperature changes of the hot months without oversizing for the unpredictable cool months.

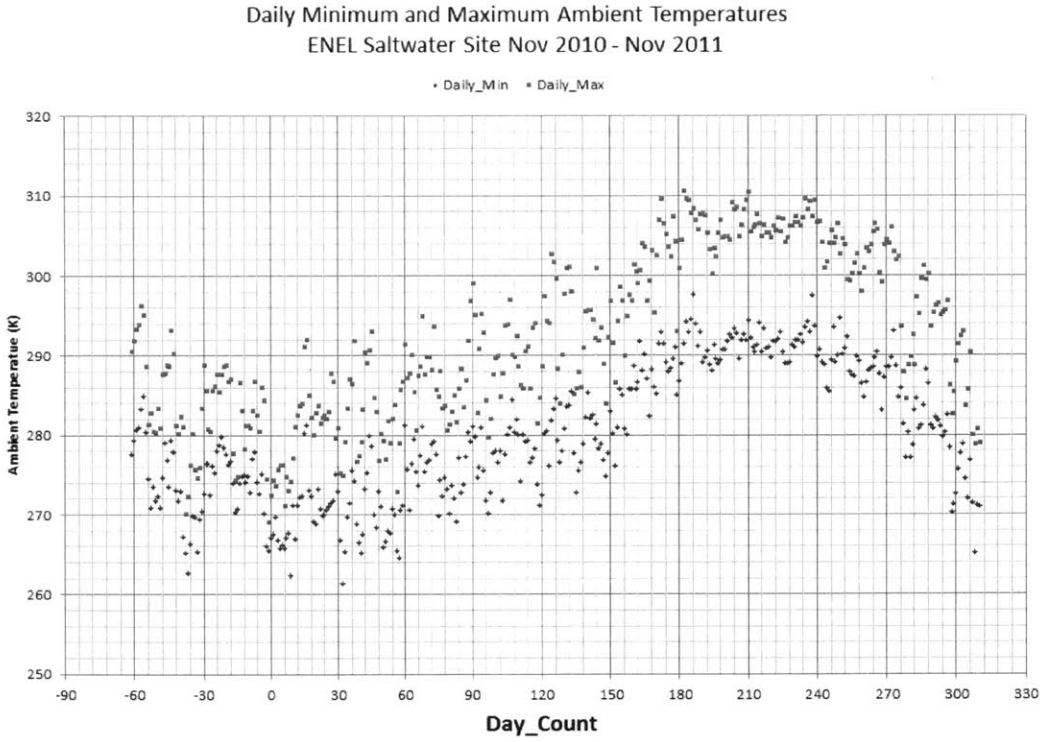

Figure 2-1: 2011 Daily Minimum and Maximum Ambient Temperature at Salt Wells Plant [5]

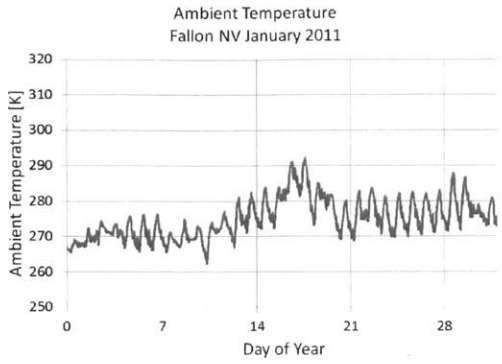

(a) Ambient Temperature January 2011

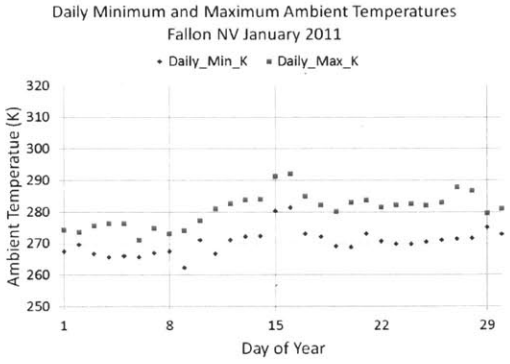

(b) Daily Min and Max Temperature January 2011

Figure 2-2: Ambient Temperature Study January 2011 Fallon Nevada [5]

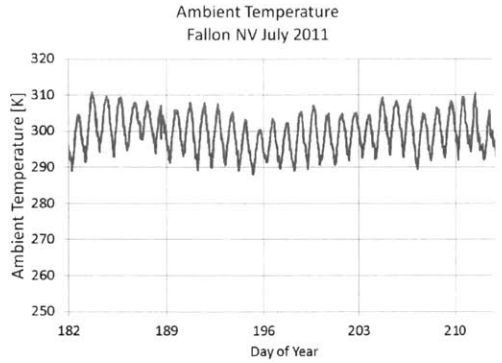

(a) Ambient Temperature July 2011

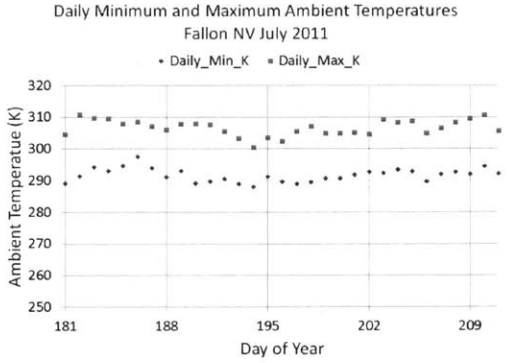

(b) Daily Min and Max Temperature July 2011

Figure 2-3: Ambient Temperature Study July 2011 Fallon Nevada [5]

For the purposes of analyzing the impact of this technology, a relatively simple control scheme is planned. The system is allowed to use the TES as the cold sink (mode 3) for a maximum of 9 hours per day. Therefore, the required capacity is set by the heat load imposed by condensing 425 kg/sec of Isobutane during the 9 hours between 11am and 8pm. These hours tend to be the hottest and also correspond to the highest electrical demand and wholesale prices.

The capacity estimation assumes that the thermal storage medium starts and ends at a homogeneous temperature. This is not the case during a transient over a finite time period. The material closest to the pipe undergoes a greater temperature change than the material furthest from the pipes. In order to roughly compensate for this the proposed system is over-sized by designing it for 12 hours of capacity. This assumption may result in a TES with excess storage capacity. In this case, a finding of insufficient system performance is that much more significant.

The operating pressure of isobutane in the condenser ranges from 300 to approximately 850 kPa with the corresponding cold sink heating rate between 132 MW and 151 MW. For sizing purposes an intermediate value of 142 MW is assumed. Concrete is the chosen storage medium and an allowable temperature change of approximately 10K is assumed based on allowable performance rollback with increased oil temperature. The results of the required storage volume calculation are shown in Table 2.1.

$\dot{Q}_{condensing}$	142 MW
time	12 hrs
$T_2 - T_1$	$10K$
$\rho_{concrete}$	$2300\frac{kg}{m^3}$
$C_{concrete}$	$960\frac{J}{kg \cdot K}$
$V_{concrete}$	279,000 m^3

Table 2.1: TES Rough Sizing

With the concrete volume established, the effects of the detailed geometry are studied. A brute force method is employed to analyze the performance impact of pipe diameter, pipe length and flow Reynolds number. Parametric sweeps are performed

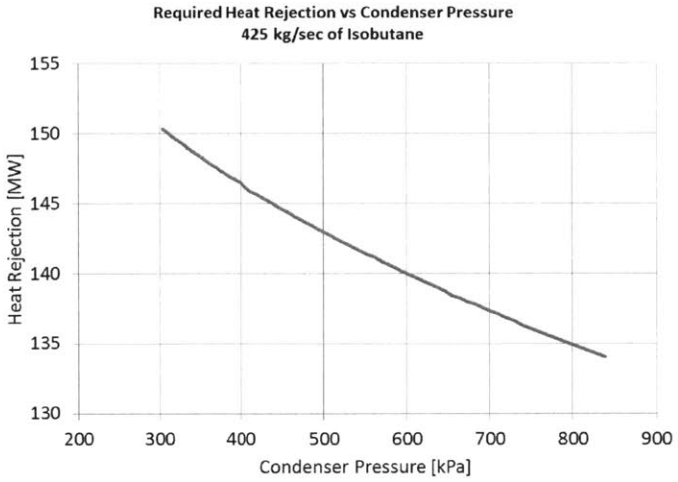

Figure 2-4: Cooling Load Required to Condense 425 kg/sec of Isobutane

over pipe diameters between 1 cm and 1 m, pipe lengths from 250 m to 5 km and Reynolds numbers from 250 and 25,000. All sweeps are performed assuming an oil mass flow rate of 10,000 kg/sec. The following calculations are performed for each combination of these variables as follows.

The flow properties for each pipe and flow configuration are established for candidate Reynolds numbers and pipe diameters. The required pipe count is then established based on the mass flow rate through each individual pipe.

$$v_{oil} = \frac{Re\mu}{\rho D_h}$$

$$\dot{m}_{oil-pipe} = \rho v_{oil} \frac{\pi}{4} D_h^2$$

$$n_{pipes} = \lceil \frac{\dot{m}_{oil-total}}{\dot{m}_{oil-pipe}} \rceil$$

For preliminary sizing, all fluid properties are taken at 310 K because this is near the expected maximum operating temperature. The oil viscosity decreases with temperature. Therefore, the oil mean velocity decreases and required pipe count increases with increasing fluid temperature at a fixed Reynolds number. Material property curves may be found in the appendix.

Calculation of Darcy friction factor and Nu for selected Re:

Internal laminar flow $Re < 2300$ [3, p761]

$$f = \frac{64}{Re_D}$$

$$Nu = 1.86 \cdot \left(Re \cdot Pr \cdot \frac{D_h}{L_{pipe}} \right)^{\frac{1}{3}} \cdot \left(\frac{\mu}{\mu_w} \right)^{0.14}$$

Internal Transition Flow $2100 < Re < 10^4$

Darcy friction factor for transition flow assumed to follow turbulent equation:

$$f = (0.790 \cdot \ln Re_D - 1.64)^{-2}$$

$$Nu = 1.116 \cdot \left(Re^{\frac{2}{3}} - 125 \right) \cdot Pr^{\frac{1}{3}} \cdot \left(\frac{\mu}{\mu_w} \right)^{0.14} \cdot \left(1 + \left(\frac{D_h}{L_{pipe}} \right)^{\frac{2}{3}} \right)$$

Internal turbulent flow $10^4 < Re < 5 \cdot 10^6$ [3, p761]

$$f = (0.790 \cdot \ln Re_D - 1.64)^{-2}$$

$$Nu = \frac{\left(\frac{f}{8}\right) (Re_D - 1000) Pr}{1 + 12.7 \left(\frac{f}{8}\right)^{\frac{1}{2}} \left(Pr^{\frac{2}{3}} - 1 \right)}$$

Calculation of convective heat transfer coefficient between fluid bulk temperature and wall temperature:

$$c = \frac{Nuk}{D_h}$$

Calculation of concrete dimensions:

$$A_{solid} = \frac{V_{concrete}}{L_{pipe} n_{pipes}}$$

$$D_o = \sqrt{\frac{4A_{solid}}{\pi} + D_h^2}$$

The average difference between the fluid bulk temperature and the pipe wall temperature is a function of the operating TES oil flow rate, the solid and oil heat capacities and the transient characteristics of the whole system. Analysis of the tran-

sient $\Delta T = T_{fluid} - T_{solid}$ is too complex to be useful during initial sizing. However, a minimum required ΔT is easily calculated as a function of the required temperature drop across the axial length of each pipe: ΔT_{axial}. This temperature drop is equal to the temperature drop across the oil cooled condenser, which is a function of the total oil mass flow and the condenser average operating pressure.

$$\Delta T_{axial} = \frac{\dot{m}_{isobutane} h_{fg-avg-isobutane}}{\dot{m}_{oil-total} C_{p_{oil}}}$$

$$\frac{\partial T}{\partial x} = \frac{\Delta T_{axial}}{L_{pipe}}$$

The ΔT is calculated once using the convective heat transfer coefficient, c, to determine the temperature difference between the liquid bulk and wall surface temperature and once using the combined convective and conductive heat transfer coefficient U for the required difference between the liquid bulk and solid bulk temperature.

$$\Delta T_{conv} = \frac{\frac{\partial T}{\partial x} V_{oil} \rho C_{p_{oil}} \frac{\pi}{4} D_h^2}{h \pi D_h}$$

$$\Delta T_U = \frac{\frac{\partial T}{\partial x} V_{oil} \rho C_{p_{oil}} \frac{\pi}{4} D_h^2}{U \pi D_h}$$

The local Biot number is used as an indicator of the transient behavior of the concrete. This local Biot number is calculated for a planar section of the pipe cut perpendicular to the axis.

$$L_c = \frac{A_{cross-section}}{\pi D_h}$$

$$Bi = \frac{h L_c}{k}$$

The required oil pumping power is estimated as a function of the oil volumetric flow rate and the pressure drop across the TES unit. The actual simulation tracks the pumping power as a function of the volumetric flow rate and the pressure drop across both the TES and the ACHX.

$$\frac{\partial p}{\partial L} = \frac{f \cdot \rho V_{oil}^2}{2D_h^2}$$

$$\Delta p_{pipe} = \frac{\partial p}{\partial L} \cdot L_{pipe}$$

$$\dot{V}_{oil-total} = \frac{\dot{m}_{oil-total}}{\rho_{oil}}$$

$$\dot{W}_{TESPump} = \dot{V}_{oil-total} \Delta p_{pipe}$$

The capital cost of a given configuration is estimated by the cost of the concrete and iron pipes required to build it. For these purposes a concrete cost of $50 per cubic meter and an iron cost of $400 per ton. [2]

The following equation is used to relate pipe thickness to its diameter. The actual thickness of the metallic pipe is variable. This exponential relationship between diameter and pipe wall thickness is intended to represent the increased wall thickness likely required for a larger pipe diameter. While the thickness values are close to the expected values of actual pipes that may be used, it is more important to capture the expected trend of sub-linear thickness increase with pipe diameter increase. This tries to ensure that competing potential configurations with different pipe diameters are not unjustly penalized by assuming a constant or linear wall thickness.

$$thk_{pipewall} = 0.01 D_h^{0.3}$$

The cross section and required iron mass of a given iron pipe configuration is calculated with diameter and wall thickness.

$$A_{pipewall} = \frac{\pi}{4}\left((D_h + thk_{pipewall})^2 - D_h^2\right)$$

$$m_{iron} = A_{pipewall} n_{pipes} L_{pipes} \rho_{iron}$$

$$CC = V_{concrete} \cdot MP_{concrete} + m_{iron} \cdot MP_{iron}$$

Test configurations are chosen for comparison trials based on the lowest cost configuration that satisfies certain constraints on ΔT_h , $\dot{W}_{OilPump}$ and Bi. Comparison

between several potential configurations yielded the following configuration.

2.2 TES Simulation with COMSOL® Multiphysics

The concrete thermal storage block is simulated by a 2D axi-symetric model in COMSOL Multiphysics ® Version 4.2a. [1] The model utilizes the Heat Transfer in Fluids module with Heat Transfer in Solids added to the simulation to represent the concrete. The model geometry consists of two concentric cylinders; the inner representing the fluid domain and the outer the solid.

Heat exchanger oil flows in one direction when the system is cooling the concrete block and the opposite direction when the concrete block is being used as the cold sink. One end of the block is designated as the hot side and one is the cold side. When the TES is used to cool the OCC (mode 3), hot oil at OCC exit temperature enters the hot side, flows through the block and exits the cold side. The bulk temperature at the cold side exit is calculated by COMSOL and is passed to the main program as the OCC inlet temperature. Conversely, when the ACHX is active (mode 2) the TES oil flows from the cold side towards the hot side. The bulk temperature at the hot side exit is the inlet temperature of the ACHX.

The outer surface of the concrete is modeled as insulated. In reality this surface is in contact with the adjacent pipe/concrete pairs. The insulation boundary condition acts to enforce the symmetry present in such a configuration.

Built in material properties for heat exchanger oil and concrete are utilized. The built in material properties are described in detail in Section 2.5.3. The built in concrete model requires a user defined specific heat capacity. This is set to a constant $C_{P_{concrete}} = 960 \frac{J}{kg-K}$. The oil density for the built in model is a function of temperature. Conservation of mass and the assumption of a constant velocity distribution necessitates a constant density of $\rho_{oil} = 875 \frac{kg}{m^3}$.

COMSOL has some difficulty efficiently modeling turbulent flow. The primary purpose of the transient simulation is to simulate the heat transfer from the TES fluid to the TES thermal storage medium. Fluid mechanics effects such as the pressure drop

along the pipe length are secondary and are adequately approximated with literature equations. Therefore, solution of the Navier-Stokes equations is ignored and the oil is modeled as constant velocity plug flow.

Lizarraga-Garcia and Mitsos have developed a technique by which turbulent heat transfer is accurately modeled in COMSOL using fixed velocity plug flow. [7] In order to ensure appropriate heat transfer characteristics in this regime, the value of the convective heat transfer coefficient, c, is matched to literature values. To accomplish this a control volume is built into a test model. For a given geometry and Reynolds number, the test model is configured to the appropriate dimensions and flow velocity and run through an example cooling cycle. The COMSOL integral tool is utilized to sum the energy flowing into and out of the control volume. The effective convective heat transfer coefficient is determined from the net heat flux with the wall and the average control volume wall temperature. For each configuration tested the oil thermal conductivity is adjusted such that the effective thermal conductivity in the fluid appropriately represents the effective thermal conductivity in a turbulent flow. This yields an $c_{effective}$ that matches the literature value for the convective heat transfer coefficient.

$$c_{effective} = \frac{\dot{Q}_{oil-in} - \dot{Q}_{oil-out}}{\pi D_h L_{CV} \left(T_{bulk-oil-CV} - T_{wall}\right)}$$

2.2.1 Metallic Pipes in TES Storage Block

The presumed metallic pipes necessary in the actual system are not modeled in COMSOL. The radial thermal resistance of such pipes is insignificant in comparison to the thermal resistance of the much thicker concrete that has a much lower thermal conductivity. See example calculations below.

$$R_{Cylinder-Conduction} = \frac{\ln\left(\frac{D_{outer}}{D_{inner}}\right)}{k2\pi}$$

A similar analysis of the axial conduction shows that the parallel resistances of

D_{hpipe}	0.66 m
thk_{pipe}	.011 m
$D_{outer-concrete}$	1.155 m
$k_{concrete}$	$1.8\frac{\mathrm{W}}{\mathrm{m \cdot K}}$
k_{iron}	$80\frac{\mathrm{W}}{\mathrm{m \cdot K}}$
$R_{iron-pipe}$	$6.52\mathrm{e}{-05}\frac{\mathrm{m \cdot K}}{\mathrm{W}}$
$R_{concrete}$	$4.66\mathrm{e}{-02}\frac{\mathrm{m \cdot K}}{\mathrm{W}}$

Table 2.2: Radial Pipe Resistance Comparison

the iron pipe and the concrete are of the same order of magnitude as the concrete alone. This indicates that the overall axial conduction rate is not largely affected by the presence or absence of the metallic pipe material. Therefore, it is assumed that the iron pipes may be neglected in the COMSOL analysis.

2.2.2 Mesh Density Studies

The density of the finite element mesh must be sufficient to preclude any adverse affects on the analysis. For example, if the mesh is too coarse the transient accuracy is diminished and if the mesh is too fine the analysis takes an unnecessarily long time to run. For this analysis, increased simulation speed is only pursued if it does not adversely affect accuracy.

In order to set the model mesh density a simulated 24 hour test run is used to exercise several potential mesh configurations. The test run includes both rapid and slow transient elements from 1 hour duration to 8 hours duration and it varies the inlet temperature over a range of 20 K. This closely approximates the transients that occur under operating conditions.

First the radial mesh density is studied. A very fine axial mesh is established with axial nodes 0.25 m apart along a 5000 m pipe length. The first axial mesh configuration has two elements through the concrete thickness and two from the pipe wall to the fluid center (axis of the pipe). The example transient run is executed and the outlet temperature at 24 hours is recorded. This process is repeated with 3+3 radial elements, 4+4 radial elements and so on until the final temperature is seen to

change less than 0.0025% for each additional element. The final radial mesh density is set to 6 elements through the concrete and 6 from the pipe wall to the center of the fluid.

Next the axial mesh density is examined. The 6+6 radial mesh is maintained and the first test is run for a slightly more coarse axial mesh than was used for the radial study. The axial element size is increased until doubling the element size is found to change the final outlet temperature by greater than 0.0025%. The axial element length is set to 25 m. This corresponds to 200 elements along the length of a 5000 m pipe. For this element length the outlet temperature after the 24 hour test run differs by 0.0031% with respect to a 0.25 m element size.

2.3 Matlab® with COMSOL Livelink®

The air cooled condensers, oil cooled condensers and oil pump may be modeled as pseudo-steady-state. Justification for this assumption is provided for each component in Section 2.4.1. The governing equations and lookup tables for their operation are modeled as Matlab functions. These functions are called as Matlab steps through simulated operation of the heat rejection and TES components at pre-defined time step intervals. Unless otherwise specified studies described are run with a 30 minute time step size.

The code is setup to run from a given start time expressed as the second of the year with zero as midnight on January 1st 2011. All of the component models are initialized to starting conditions based on the average temperature of the previous 24 hours.

At the beginning of each time step a lookup table provides the instantaneous ambient temperature. Control logic uses the ambient temperature, TES block state and the time of day to determine what operating mode should be executed. Next fan powers, pump powers, condenser pressure, turbine output and oil temperature changes are calculated using the associated Matlab functions for the given operating parameters and ambient temperature. The corresponding TES oil input temperature

is then established and finally Matlab calls COMSOL to run the TES block for a duration of one time step. The oil outgoing temperature at the end of the time step is then stored and used as the starting point for the following time step. This process continues until the desired simulation time is achieved.

2.3.1 Ambient Temperature Data

Ambient temperature as a function of time is the only required input for the system model. Fallon Nevada historical observations at 30 minute intervals are used to initialize the starting temperature of the TES and by the ACC and ACHX Matlab functions to set the incoming air temperature of the air-cooled heat exchange simulations. The simulation is only allowed to use weather data from the current time or previous time steps. The system is not allowed the benefit of weather predictions.

The effects of wind conditions, cloud cover, humidity and precipitation are neglected.

2.3.2 Operating Mode Logic

The simulation code has three primary operating modes as described in Section 1.6. The operating mode selection is made at the beginning of each time step and is based on the time of day, the TES state and a comparison between the potential power produced in potential modes. See Figure 2-5 for visual representation of the decision process.

The first consideration in the operating mode decision is the time of day. The TES is only allowed to act as a cold sink during the hours between 11am and 8pm. Between 11am and 8pm the system defaults to mode 3, condensing in the OCC with the TES as the eventual cold sink. At the beginning of each time step the potential net power generation from the OCC condensing (mode 3) and the ACC condensing (mode 1) are compared based on ambient temperature and the state of the TES block. If the net power generation from mode 1 is greater than mode 3 then the system switches to either mode 1 or 2.

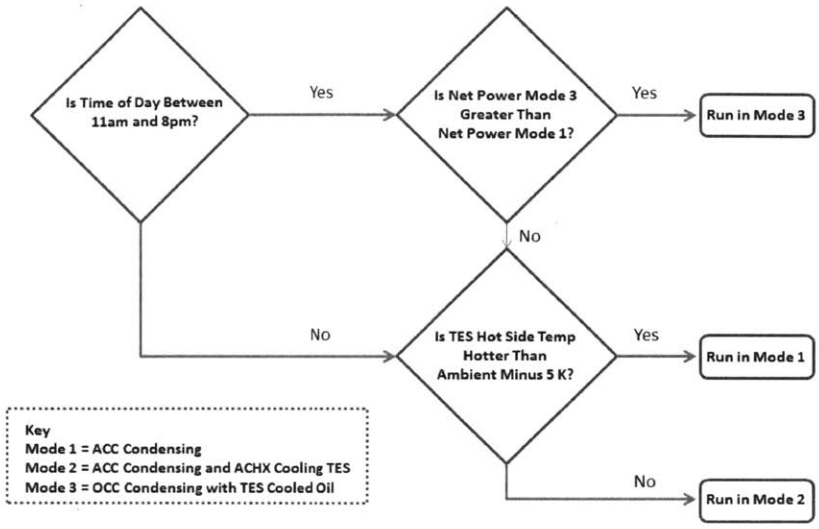

Figure 2-5: Operating Mode Decision Tree

The decision between mode 1, condensing with ACC or mode 2, condensing with the ACC and cooling the TES block with the ACHX is also made in regard to the ambient temperature and the TES state. The ACHX only runs when it is assumed to be providing more benefit to the system than it costs in parasitic load. As a rule for this analysis the ACHX is considered to be providing more benefit than it costs to run when the ambient temperature is at least 5 K lower than the TES block hot side discharge temperature. This rule is explained further in the ACHX design section.

The system is not allowed to re-enter mode 3 once it has switched from mode 3 to mode 1 in a given day. It is expected that this change in operating regime would require operator intervention and that it would be unreasonable to switch back and forth multiple times per day.

If the time step starts outside the 11am-8pm window, then the system defaults to mode 2, condensing with the ACC and cooling the TES block with the ACHX. Once again, mode 1 is employed as an alternative to mode 2 when the ambient temperature is not at least 5 K cooler than the TES block hot side discharge. In this case there is no potential to cool the TES and the ACHX is switched off to prevent unnecessary parasitic load.

It is recognized that this is likely not the optimal operating regime for a system of this type. It is the purpose of this thesis to estimate the benefits and costs of such

a system. A simplified control system is sufficient to determine gross trends.

2.4 Non-TES Heat Exchange Components Simulation and Design

2.4.1 Pseudo Steady-State Assumption for Condensers and Heat Exchangers

Before the details of the ACC, OCC and ACHX simulation are developed, it must be established that operation of these components may be modeled as pseudo steady-state. In order to understand the transient behavior of the pipes and casings of the heat exchangers, their heat exchange duty is compared to the rate of heat absorption under a typical step change in incoming fluid temperature. The condenser duty and temperature rate of change are calculated from 2011 operational data provided by ENEL.

$$\dot{Q}_{\text{condenserduty}} = \dot{m}_{\text{C4H10}} \Delta h_{\text{C4H10}}$$

The 2011 data shows an average $\dot{Q}_{\text{condenserduty}} = 133\text{MW}$

The rate of heat absorption into the pipes and casing of the heat exchange equipment of the condenser is

$$\frac{\partial E}{\partial t}_{\text{equipment}} = m_{\text{equipment}} C_p \frac{\partial T}{\partial t}$$

From ACC specifications:

Steel ACC pipes

$$M_{\text{pipes}} = 445,000\text{kg}$$

$$C_{\text{steel}} = 500 \frac{J}{\text{kgK}}$$

Aluminum Fins

$$M_{\text{fins}} = 11,283,000\text{kg}$$

$$C_{\text{aluminum}} = 900\frac{\text{J}}{\text{kgK}}$$

Under an average transient $\frac{\Delta T_{\text{inlet}}}{\Delta t}$ is $.00042\frac{\text{K}}{\text{s}}$. This results in an energy absorption rate of

$$\frac{\partial \text{E}}{\partial \text{t}}_{\text{equipment}} = 4.5\text{MW}$$

This corresponds to about 3.5% of the heat exchange duty.

An extreme transient is modeled by the mean plus 3 sigma $\frac{\Delta T_{inlet}}{\Delta t}$ of $.00245\frac{K}{s}$ for 2011. This results in an energy absorption rate of

$$\frac{\partial \text{E}}{\partial \text{t}}_{\text{equipment}} = 26\text{MW}$$

This corresponds to about 20% of the heat exchange duty.

Under normal operating conditions the equipment absorbs or rejects (depending on the direction of transient) energy at about 3.5% of it's intended heat exchange duty to equilibrate to the fluid temperature. Since this energy remains in the system it will act as a sort of time delay. Since the magnitude of the energy stored vs the overall heat duty is generally small, the effect on the transient behavior of the plant operation is negligible.

The ACHX is assumed to have the same geometry as the ACC. The OCC has a significantly smaller mass than the ACC, as it is a liquid cooled condenser and, as such, requires less surface area. Therefore the OCC is even closer to pseudo steady-state than the ACC and ACHX. The ACC, ACHX and OCC are modeled as steady-state.

2.4.2 Air Cooled Condenser Simulation

The Salt Wells ACC units are an induced draft cross flow configuration. The fluid pipes are arranged in five rows of two passes per row. The pipes are arranged such that the hot fluid enters at the topmost row where the passing air has been heated by the lower rows. This is modeled as a discretized counter flow heat exchanger with N nodes and N-1 discrete sections. The first node corresponds to isobutane entering the ACC and air exiting. The discrete simulation proceeds one section at a time until

the last node where the isobutane exits the ACC and the air enters. The simulation of the ACC counterflow heat exchange is modeled with a forward differences method. The heat exchange in each discrete section is governed by the following equations.

The heat exchange in each section is calculated by the isobutane-air temperature difference at the section node corresponsing to the isobutane inlet. The isobutane enthalpy is then calculated based on the incoming enthalpy, the section heat exchange and the mass flow rate. The outgoing isobutane enthalpy is then used to determine the outgoing isobutane phase and temperature. The change in air temperature across the section is calculated under the assumption that the air is always in the gaseous phase. Note that the air temperature at node n+1 is a smaller value than at n. This is because the air is flowing in the opposite direction as the isobutane.

$$\dot{Q}_{\text{section}} = dA \cdot U \cdot (T_{\text{isobutane}} - T_{\text{air}})$$

$$h_{\text{isobutane}_{n+1}} = h_{\text{isobutane}_n} + \frac{\dot{Q}_{\text{section}}}{\dot{m}_{\text{isobutane}}}$$

$$T_{\text{isobutane}_{n+1}} = \begin{cases} f(h,p) & \text{if } h_{isobutane_{n+1}} > h_{v_{sat}} \\ f(h) & \text{if} h_{isobutane_{n+1}} < h_{f_{sat}} \\ T_{sat} & \text{otherwise} \end{cases}$$

$$T_{\text{air}_{n+1}} = T_{\text{air}_n} - \frac{\dot{Q}_{\text{section}}}{\dot{m}_{\text{air}} \cdot C_{p_{\text{air}}}(T_{\text{air}_n})}$$

The ultimate purpose of simulating the ACC operation is to determine the isobutane pressure that can be sustained as a function of ambient temperature. A pair of nested bisection loops are employed to determine this pressure for a given ambient temperature. The correct operating pressure is achieved when the isobutane exits the ACC at 1K below the saturation temperature.

Two bisection loops are necessary because both the condenser pressure and the corresponding air outlet temperature are unknown. The outer loop bisects between the maximum and minimum pressures of 1000 kPa and 300 kPa respectively. These

values are chosen as they bracket pressures reasonable accomplished with expected ambient temperatures in the range of 260K - 315K. The inner bisection loop solves for the air exit temperature by bisecting between an upper limit of the isobutane inlet temperature and a lower limit of the air inlet temperature.

Bisection is not the most efficient numerical scheme to identify the condenser pressure and appropriate air exit temperature. However, bisection always converges to the correct value for monotonic functions. The level of subcooling varies monotonically with the condenser pressure for a given cooling capacity and the air inlet temperature varies monotonically with air exit temperature for a given condenser pressure and heat exchange duty.

Solving for the correct operation at a given ambient temperature begins by simulating the ACC operation at the average of the minimum and maximum pressures. The isobutane is assumed to always enter the ACC at 10K above saturation temperature. The bisection starting value for the air exit temperature is calculated based on the average of the isobutane and air inlet temperatures. Then the forward differences simulation of the ACC is carried out across it's effective length. If the corresponding air inlet temperature is found to differ from ambient by more than a certain tolerance, the bisection limits are moved and the simulation is repeated until the simulated air inlet matches ambient within tolerance. When this is achieved the subcooling level of the exiting isobutane is compared to the target subcooling level of 1K. If the trial subcooling level differs from the desired 1K subcooling by more than an allowable tolerance the bisection limits are adjusted and this process is repeated until the prescribed 1K of subcooling is achieved.

The effective heat transfer coefficient, U, is an integral part of the forward differences condensation simulation. The value of U is a function of the heat exchanger geometry, air flow rate, isobutane flow rate and whether the heat exchange is from vapor to air, two-phase to air or liquid to air. The first step in this process is calculation of the air flow rate based on an assumed fan speed and the ambient air temperature and density. This air flow rate is then used to calculate a convective heat exchange coefficient for the air side heat transfer. The liquid side convective heat exchange co-

efficients are functions of the isobutane mass flow rate and the flow regime. Finally, the two convective heat transfer coefficients are combined with a constant conduction resistance to yield U.

A byproduct of the ACC operation is the parasitic load induced on the system by the operation of the ACC fans. The power consumption of these fans depends on the selected configuration and the fan speed at any given condition. For example, the existing example plant utilizes an ACC configuration with 126 fans. One-third of the fans operate at a fixed speed and the remaining two-thirds have variable speed drives. The fans operate at maximum power unless the ACC has reached the minimum operating pressure of 300 kPa. In this case the variable speed fans are slowed until they provide just enough airflow (and thus heat transfer coefficient) to accomplish the condensation.

The equations used to calculate the convective fan power consumption, heat transfer coefficients and effective U value are based on curves and studies provided by the ACC manufacturer for the specific example plant application. Their implementation for this thesis is unique to this study, but a more detailed examination of the manufacturer curves and their relationship with traditional literature heat exchange values is examined by Ghasemi and Mitsos. [5]

The effects of the isobutane pressure drop across the ACC are ignored. Both the standard configuration and the TES enhanced configuration would have the same pumping loads when the ACC is in service. The OCC is likely to have different pressure drop characteristics than the ACC, but these loads are assumed to be negligible considering the low mass flow rate of the isobutane and the fact that these systems are specifically designed for the application.

2.4.3 ACC Fan Count

The existing Salt Wells facility utilizes a 126 fan ACC but herein 252 fans are used as the base case for a more fair comparison. Preliminary simulations of the TES enhanced system are run with a 126 fan ACC and a 126 fan ACHX. Figure 2-6 shows a net power comparison between 126 fan ACC system and a 252 fan ACC system.

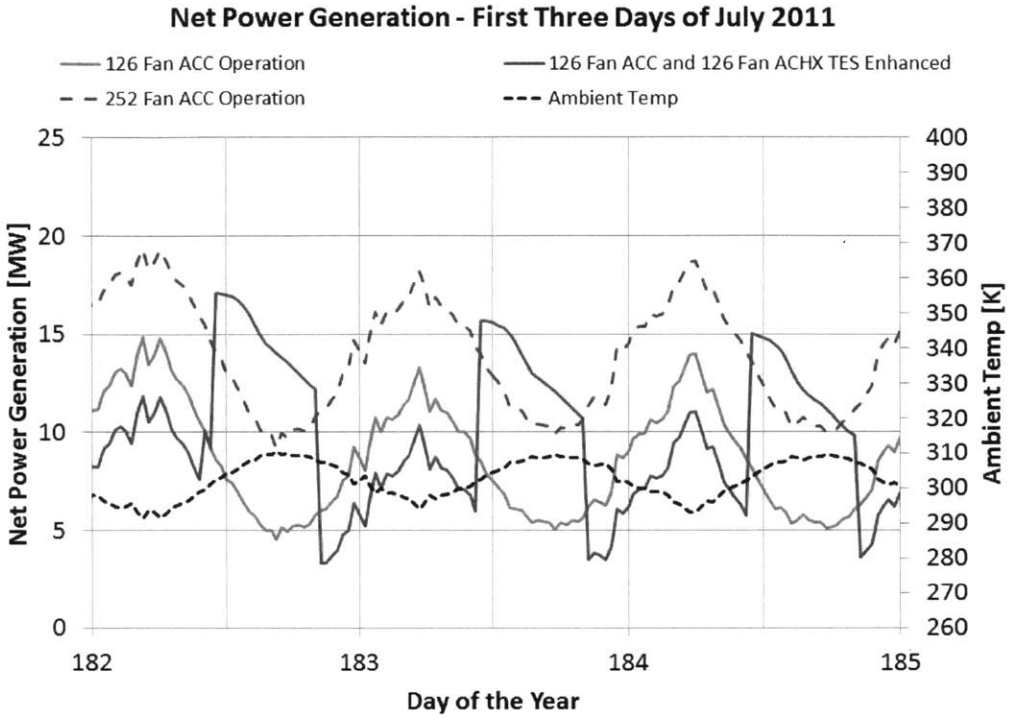

Figure 2-6: Net Power Generation for 126 Fan and 252 Fan ACC Configurations

These preliminary simulations show a dramatic energy production increase for the TES enhanced system with 126 fan ACC and a 126 fan ACHX. However, this seems to be largely due to the increased cooling capability provided by the 126 fan ACHX. Comparison to a modified configuration with a 252 fan ACC and no TES shows that the facility produces even more energy when the 126 ACHX fans are instead applied directly to cooling the ACC.

The ACC must be properly sized for summer operation in order to demonstrate the benefits of a TES enhanced system. Therefore, a modified plant model with a 252 fan ACC is adopted for comparison to the TES enhanced system. The TES enhanced air cooled heat exchangers include a 252 fan ACC and a 252 fan ACHX.

Figures 2-7, 2-8 and 2-9 show the Condenser Pressure, Turbine Gross Power and Fan Parasitic Load curves versus ambient temperature for a 126 fan ACC and a 252 Fan ACC.

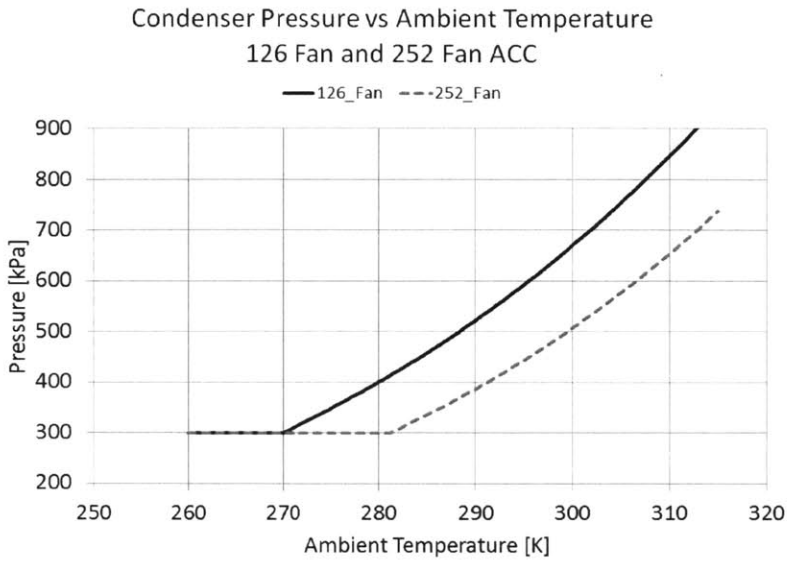

Figure 2-7: ACC Condenser Pressure vs Ambient Temperature for 126 Fan and 252 Fan ACC Configurations

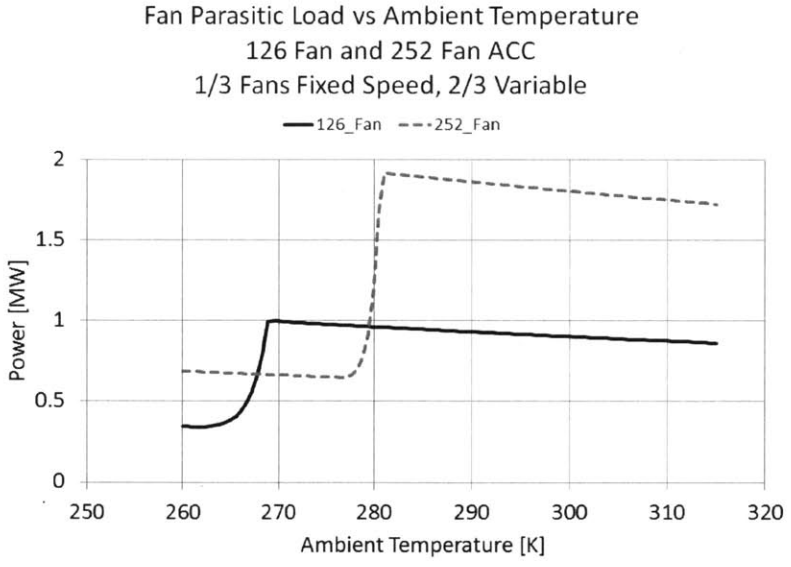

Figure 2-8: Turbine Gross Power Output vs Ambient Temperature for 126 Fan and 252 Fan ACC Configurations

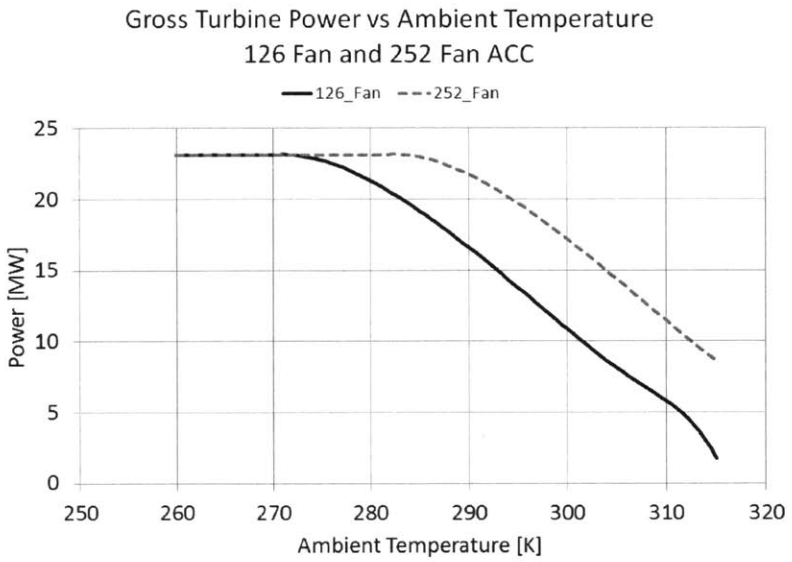

Figure 2-9: ACC Fan Parasitic Load vs Ambient Temperature for 126 Fan and 252 Fan ACC Configurations

2.4.4 Air Cooled Heat Exchanger Simulation

The simulation of the ACHX is very similar to the air cooled condenser except that the fluid side convection concerns only liquid heat exchanger oil instead of vapor, two-phase and liquid isobutane. The fan power, air flow rate and air side convective heat transfer coefficient equations for the ACHX are the same that are employed for the ACC. The oil side convective heat transfer coefficient is based on model heat exchanger oil properties and the following equations:

Calculation of Darcy friction factor and Nu for selected Re:

Internal laminar flow Re < 2300 [3, p761]

$$f = \frac{64}{Re_D}$$

$$Nu = 1.86 \cdot \left(Re \cdot Pr \cdot \frac{D_h}{L} \right)^{\frac{1}{3}} \cdot \left(\frac{\mu}{\mu_w} \right)^{0.14}$$

Internal Transition Flow $2100 < Re < 10^4$

$$f = (0.790 \cdot \ln Re_D - 1.64)^{-2}$$

$$Nu = 1.116 \cdot \left(Re^{\frac{2}{3}} - 125\right) \cdot Pr^{\frac{1}{3}} \cdot \left(\frac{\mu}{\mu_w}\right)^{0.14} \cdot \left(1 + \left(\frac{D_h}{L}\right)^{\frac{2}{3}}\right)$$

Internal turbulent flow $10^4 < Re < 5 \cdot 10^6$ [3, p761]

$$f = (0.790 \cdot \ln Re_D - 1.64)^{-2}$$

$$Nu = \frac{\left(\frac{f}{8}\right)(Re_D - 1000)\,Pr}{1 + 12.7\left(\frac{f}{8}\right)^{\frac{1}{2}}\left(Pr^{\frac{2}{3}} - 1\right)}$$

Calculation of convective heat transfer coefficient between fluid bulk temperature and wall temperature:

$$c = \frac{Nuk}{D_h}$$

The required oil pumping power for the ACHX is estimated as a function of the oil volumetric flow rate and the pressure drop across the ACHX unit. The value of $\frac{\partial p}{\partial L}$ is calculated for each section along the forward differences heat transfer simulation in the ACHX function. The average value $\left(\frac{\partial p}{\partial L}\right)_{avg}$ is then used to calculate the pressure drop.

$$\frac{\partial p}{\partial L} = \frac{f \cdot \rho V_{oil}^2}{2D_h^2}$$

$$\Delta p_{ACHX} = \left(\frac{\partial p}{\partial L}\right)_{avg} \cdot L_{ACHX}$$

$$\dot{V}_{oil-total} = \frac{\dot{m}_{oil-total}}{\rho_{oil}}$$

$$\dot{W}_{TESPump} = \dot{V}_{oil-total} \Delta p_{pipe}$$

2.4.5 Air Cooled Heat Exchanger Operating Logic

An attempt is made at assigning a value to the ACHX operation in order to efficiently control when the ACHX is active. The primary consideration for this analysis is establishing a relationship between additional work that can be done at a later time as a result of running the ACHX and the current operating conditions.

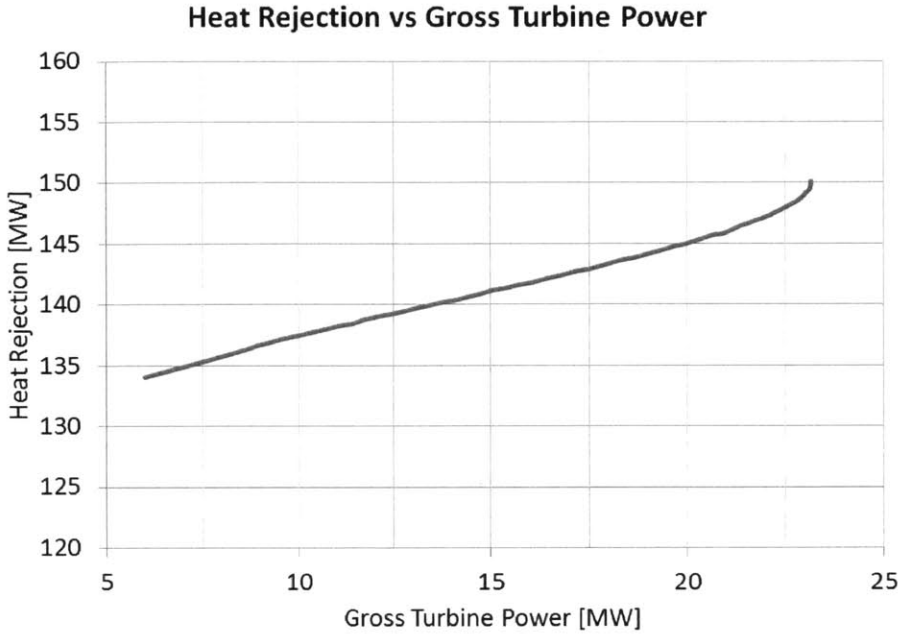

Figure 2-10: Heat Rejection vs Turbine Gross Output

The first step in this assessment is assigning a value to a given ACHX heat rejection. Figure 2-10 shows the required heat rejection vs gross turbine power for the example plant. This plot is a combination of the gross turbine power vs condenser pressure and heat rejection vs condenser pressure characteristics of Figures 1-6 and 2-4. Figure 2-11 shows the ratio of heat rejection to turbine gross power for the operating condenser pressure range. Between 6 and 22 MW must be rejected to the cold sink for every 1 MW of power generated. Therefore, every 1 MW required to run the ACHX should be accompanied by at least 6 to 22 MW of cooling. For the purposes of this rough analysis a threshold value of 11 MW cooling per MW turbine power is chosen.

Figure 2-12 shows the ACHX required fan power versus the temperature difference between the TES hot side discharge (ACHX inlet) and the ambient temperature. This data is from a one year trial run of the TES enhanced system model that is allowed to use the ACHX if the TES hot side discharge is at least ambient temperature. The ACHX parasitic load is between 1.75 and 2.05 MW with a slight positive correlation between parasitic load and temperature differential. This correlation is likely due to

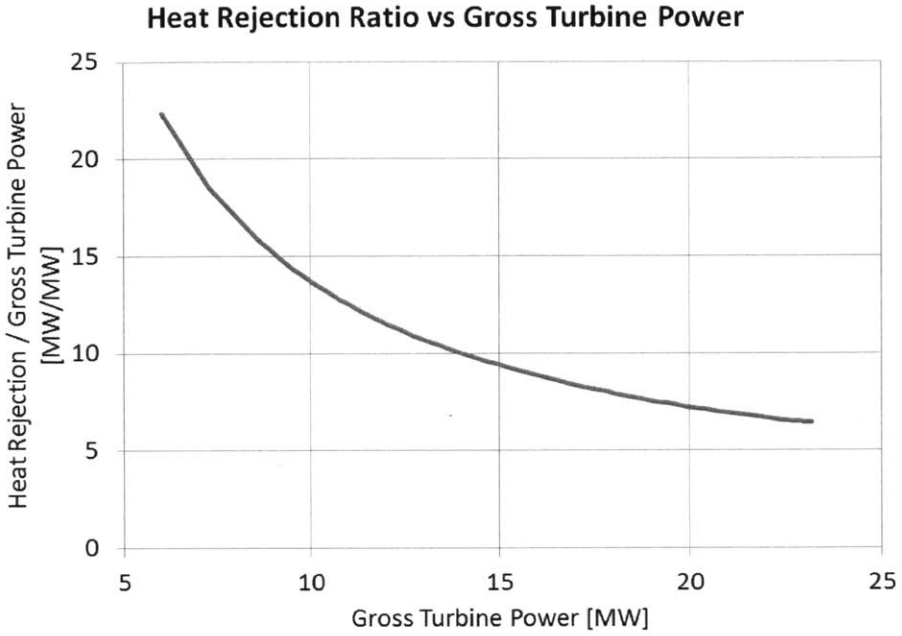

Figure 2-11: Heat Rejection Ratio vs Gross Turbine Power

the fact that higher temperature differentials are more likely to occur on cold days when the air is more dense and higher fan motor power is required.

Figure 2-13 shows ACHX heat rejection capability as a function of the temperature differential between the TES hot side and ambient temperature. In order to store at least enough cooling capacity to make up for 2 MW of parasitic load from the ACHX, at least 22 MW of heat rejection is required. This corresponds to approximately a 5K temperature differential between the TES hot side discharge and the ambient temperature. A rule in the operating logic requiring a 5K temperature differential between the TES hotside discharge and ambient is enforced in the final run of the system model presented in the results section.

2.4.6 Oil Cooled Condenser Simulation

The OCC model is a combination of the air cooled condenser and the air cooled heat exchanger. The key difference is that the OCC has no variable air flow, fan speed or dependence on ambient temperature. The OCC uses the vapor, two-phase and liquid isobutane logic from the ACC and the oil side equations from the ACHX.

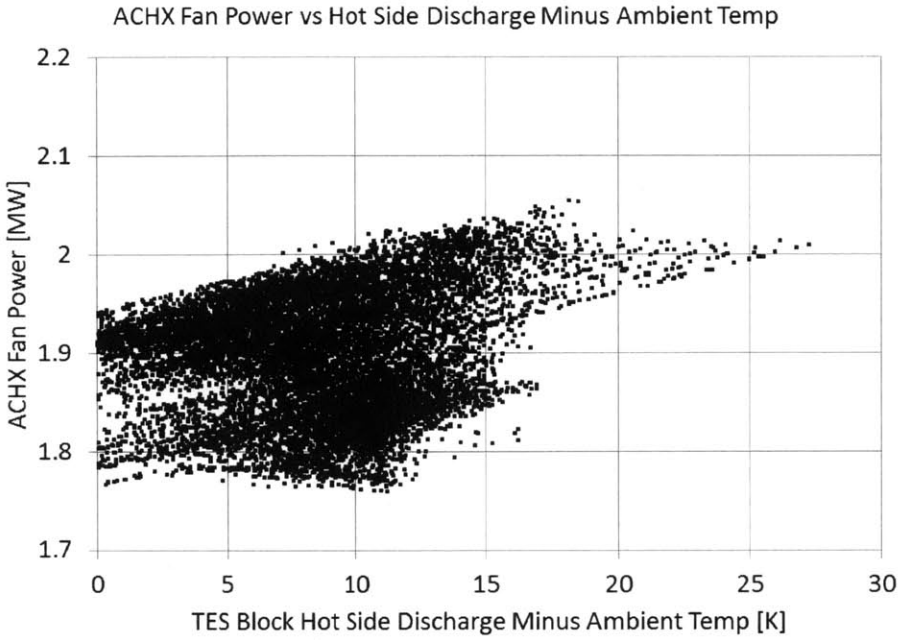

Figure 2-12: Power Required to Drive ACHX

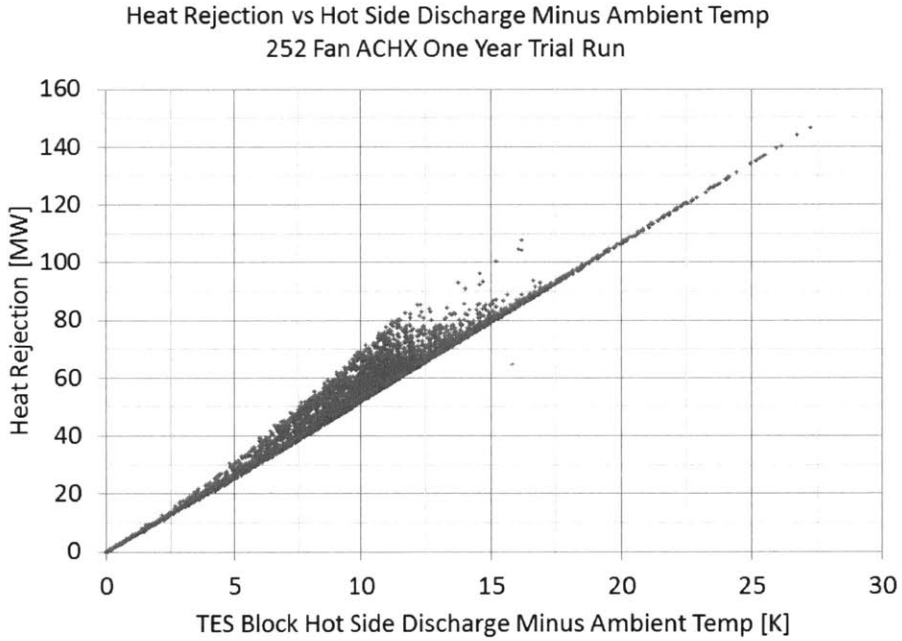

Figure 2-13: ACHX Heat Rejection vs TES Hot Side Discharge Minus Ambient Temp

Both the isobutane flow rate and the oil flow rate are fixed for all time points, so the achievable condensing pressure is a function of the incoming oil temperature for a given configuration.

2.5 Oil Cooled Condenser Sizing Studies

The OCC heat exchange surface area and oil flow rate are the key parameters that govern its behavior. Figure 2-14 shows the effect of the heat exchange area on the condenser pressure profile for a fixed oil flow rate. Additional area beyond 100,000 m^2 offers rapidly diminishing returns. Figure 2-15 shows the minimum approach temperature profile as a function of OCC area. This demonstrates that areas over 100,000 m^2 have negligible approach temperatures. The OCC system is modeled with an OCC heat exchange area of 100,000 m^2.

Selection of the oil flow rate is determined based on a simplified analysis of four key operating points. The first two time points are the beginning and end points of the oil cooled condensing phase of operation. The third anf fourth time points examined are the beginning and end of the air cooling of the oil and TES block. The simplified analysis is conducted assuming a constant ambient temperature of 300K, a TES block temperature migration of 10K, a 252 fan ACHX model and an OCC model with an area of 100,000 m^3. Figure 2-16 shows the anticipated turbine power as a function of mass flow rate with oil cooled condensing for OCC incoming temperatures of 305K and 315K. This corresponds to a starting point at 5K above ambient and an additional 10K due to the TES block migration. This figure indicates that anything over 10,000 $\frac{kg}{s}$ shows diminishing returns that may not be worth the additional pumping power.

Figure 2-17 shows the heat rejection rates for the beginning of the simplified ACHX cooling cycle. The ACHX oil inlet temperature at time 3 is assumed to be the OCC outlet temperature from time 2. Determining the actual end point ACHX inlet temperature at time 4 requires detailed understanding of the TES block and ACHX dynamics. Therefore, it is assumed that the 10K TES block migration temperature

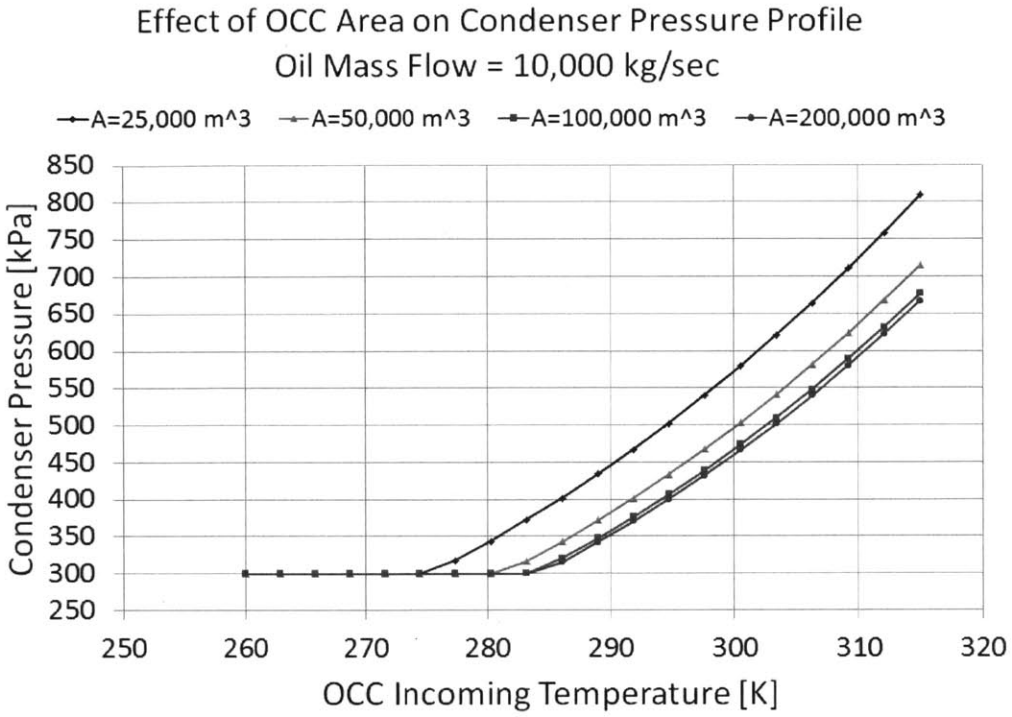

Figure 2-14: Effects of Heat Exchange Area on Oil Cooled Condenser Pressure Profile

is achieved regardless of the oil mass flow. In spite of this simplification, the results of this analysis are instructive. Once again the benefit of increased oil mass flow rate starts to show diminishing returns at 10,000 $\frac{\text{kg}}{\text{s}}$. Recall that at least 22 MW of heat rejection is necessary to justify operating the ACHX at 10,000 $\frac{\text{kg}}{\text{s}}$ oil flow rate. The time 3 heat rejection rate for 20,000$\frac{\text{kg}}{\text{s}}$ barely exceeds that of 10,000$\frac{\text{kg}}{\text{s}}$ by this amount. Since this is likely the maximum heat rejection condition, the additional oil flow rate is unnecessary and likely detrimental. All full simulations are therefore executed assuming an oil flow rate of 10,000$\frac{\text{kg}}{\text{s}}$.

Figures 2-18 shows the gross turbine power than can be accomplished when condensing with 10,000 $\frac{\text{kg}}{\text{s}}$ in an OCC with 100,000 m^2 heat exchange area. Figure 2-19 shows the corresponding OCC outlet temperatures as a function of oil inlet temperature. These curves are valid regardless of ambient temperature when the plant is operating in mode 3. Therefore, they are implemented as lookup tables in the Matlab code.

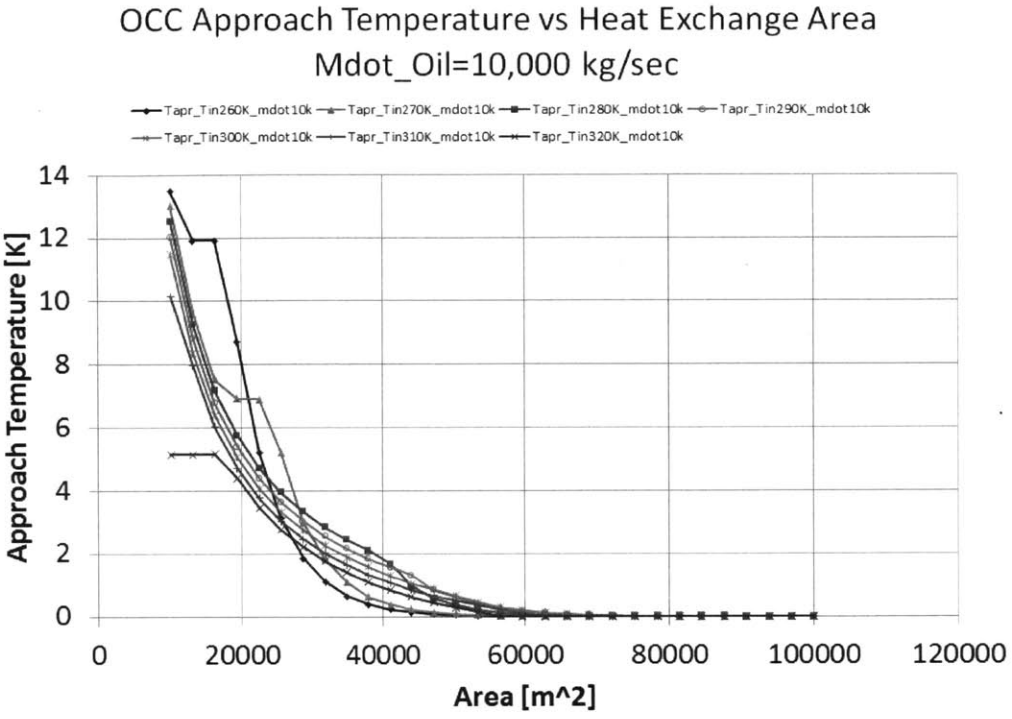

Figure 2-15: OCC Approach Temperature vs Heat Exchange Area

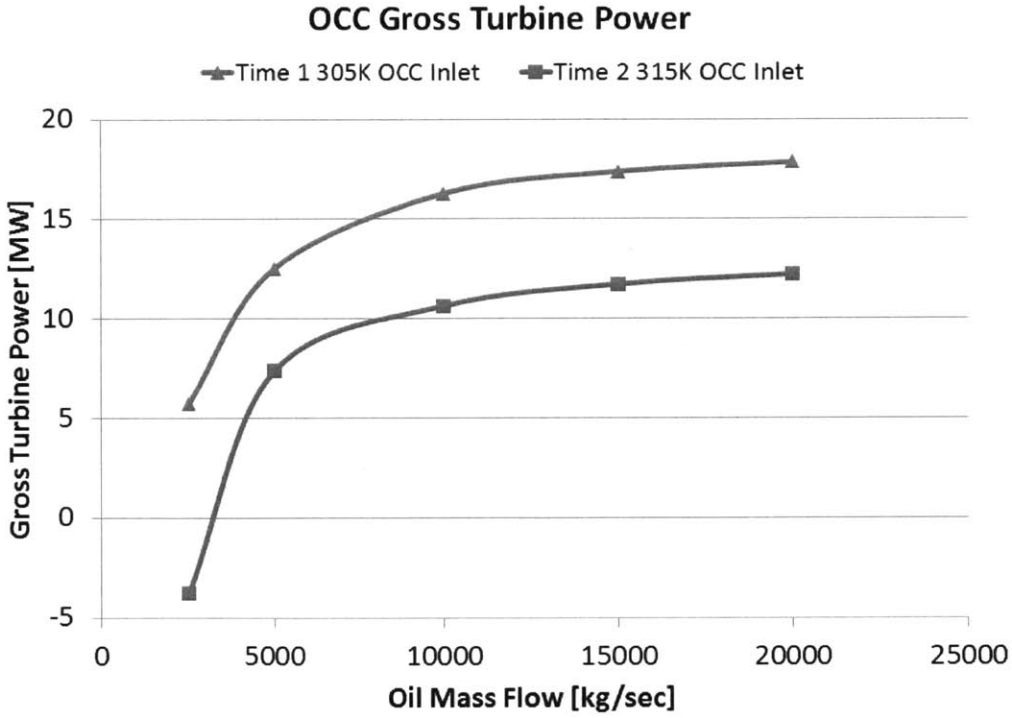

Figure 2-16: Oil Mass Flow Study - Simplified Oil Cooled Condensing Cycle Power Generation

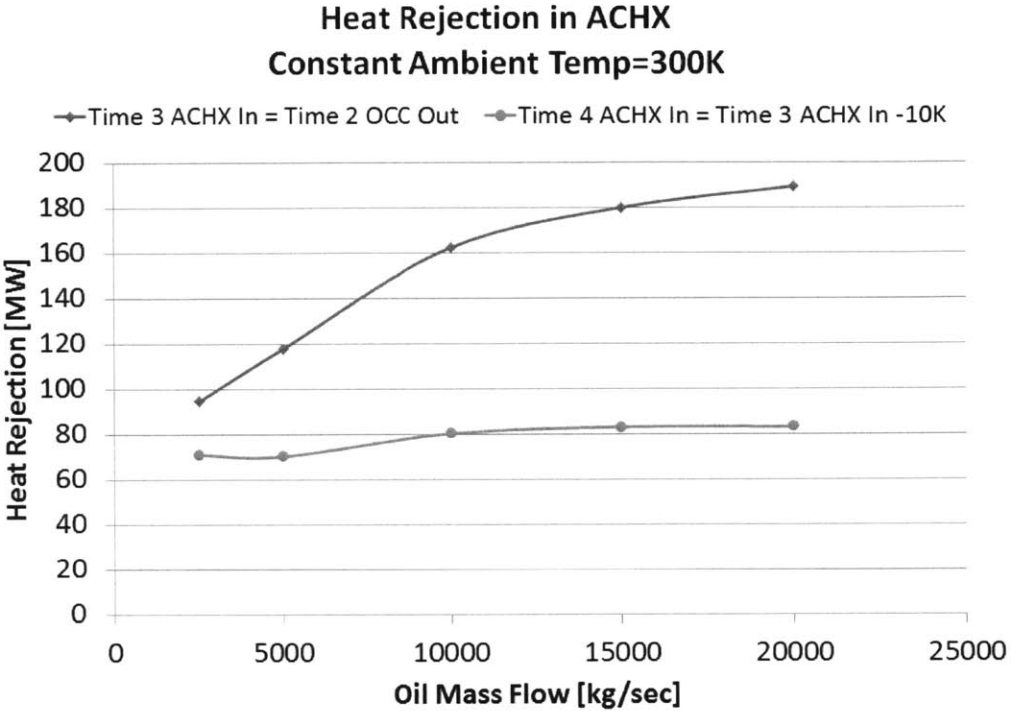

Figure 2-17: Oil Mass Flow Study - Simplified Cooling Cycle Heat Rejection

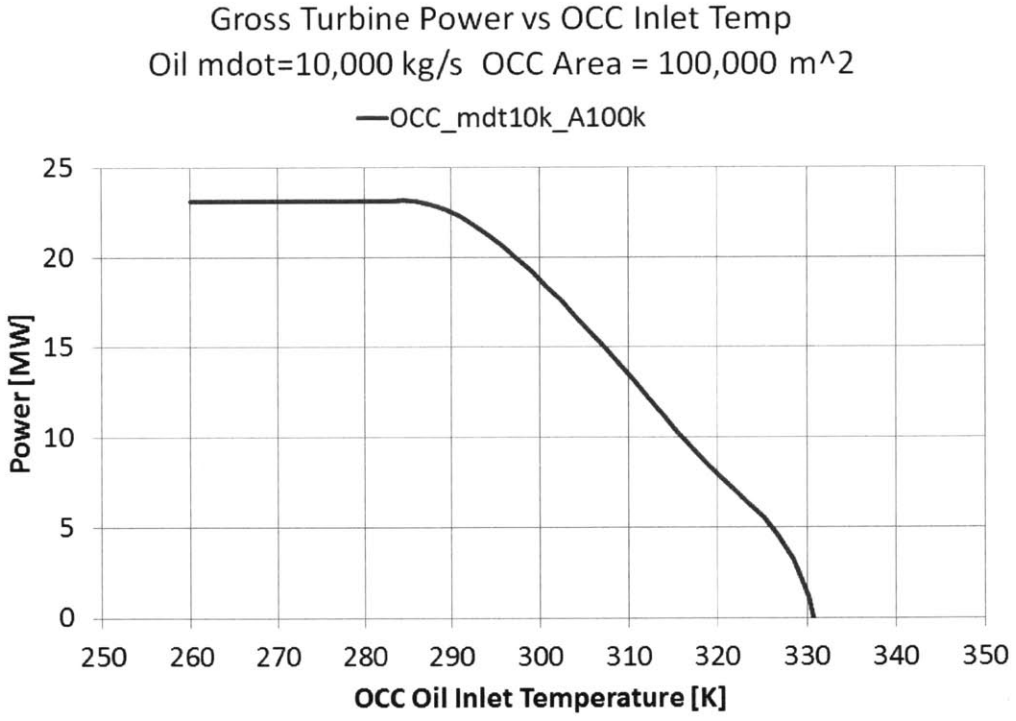

Figure 2-18: Power Generation During Oil Cooled Condenser Operation

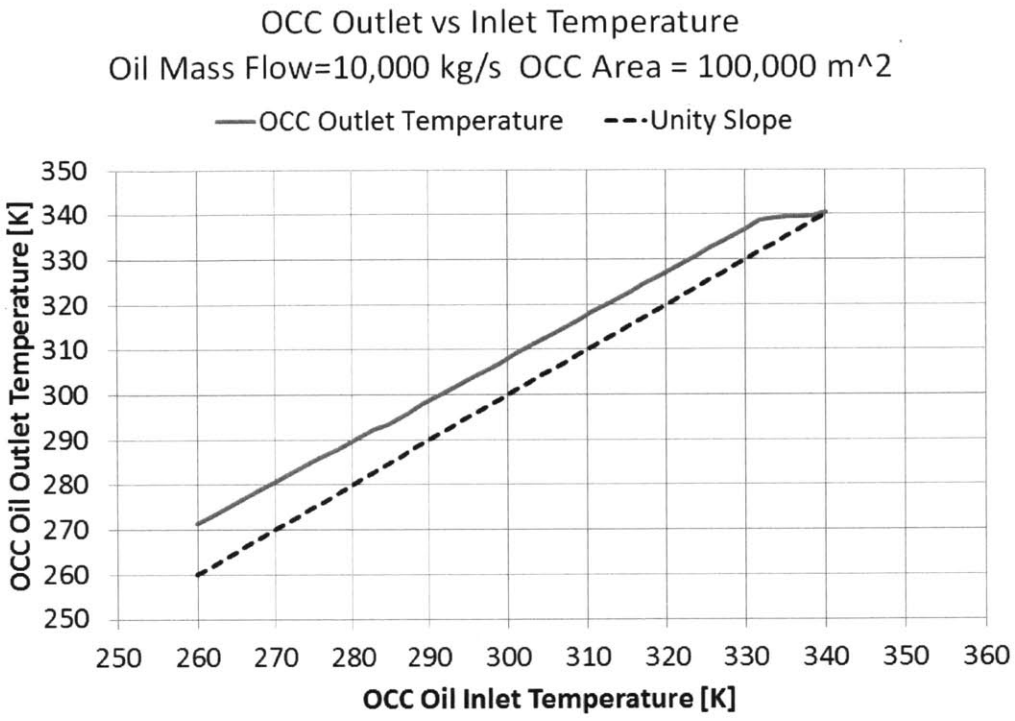

Figure 2-19: Oil Cooled Condenser Outlet vs Inlet Temperature

2.5.1 Isobutane Model

Isobutane property models are based on the RefProp®material database provided by the U.S. National Institute of Standards and Technology (NIST). [8] Isobutane properties are required for vapor, two phase and liquid isobutane.

An interpolation table is used to establish the isobutane enthalpy, as a function of prescribed pressure and temperature, at the condenser inlet. Another interpolation table is used to determine the temperature of the superheated vapor as a function of pressure and enthalpy. See Figure 2-20 for a plot of this data.

Interpolation tables are developed for the saturation temperature, enthalpy of saturated liquid and enthalpy of saturated vapor as a function of condenser pressure. This data is used to determine the condenser inlet temperature (10 K above saturation temperature as an operating rule), when the isobutane has transitioned from vapor to two-phase, the temperature of the two phase flow and when the isobutane transitions from two-phase to liquid.

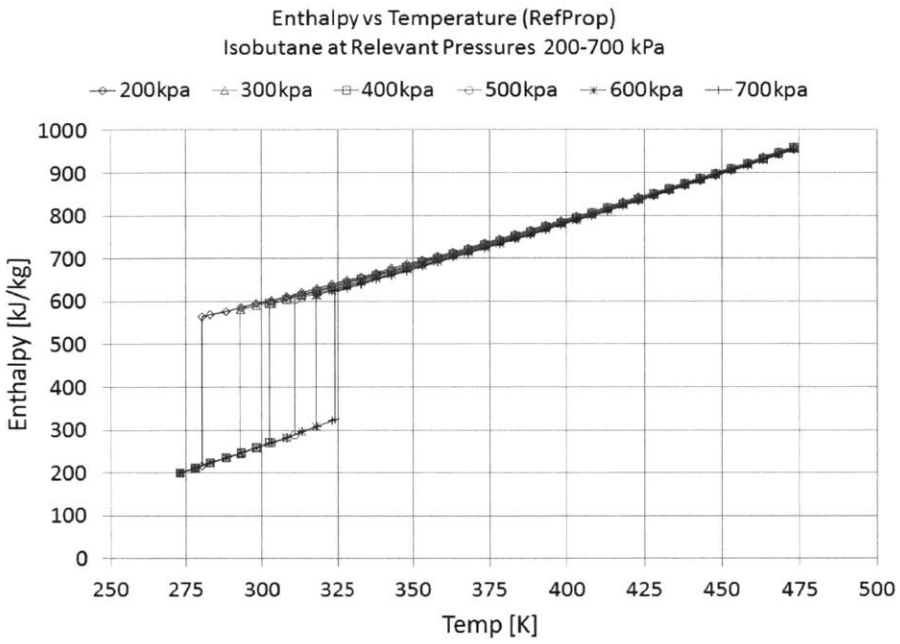

Figure 2-20: Isobutane Enthalpy as a function of Temperature and Pressure

The values of enthalpy as a function of temperature are found to fall on a line regarless of pressure in the range of interest. Therefore, the temperature of the liquid isobutane is calculated from a function derived from a linear regression of the liquid isobutane enthalpy data.

2.5.2 Air Model

The ACC and ACHX simulations require models of the specific heat capacity and density of air as a function of temperature. This data is extracted from RefProp [8] and developed into interpolation tables. Figure 2-21 shows the specific heat of air at the plants atmospheric pressure of approximately 87.5 kPa (plant altitude is 4000 feet above sea level). Figure 2-22 shows the density as a function of temperature for 87.5 kPa.

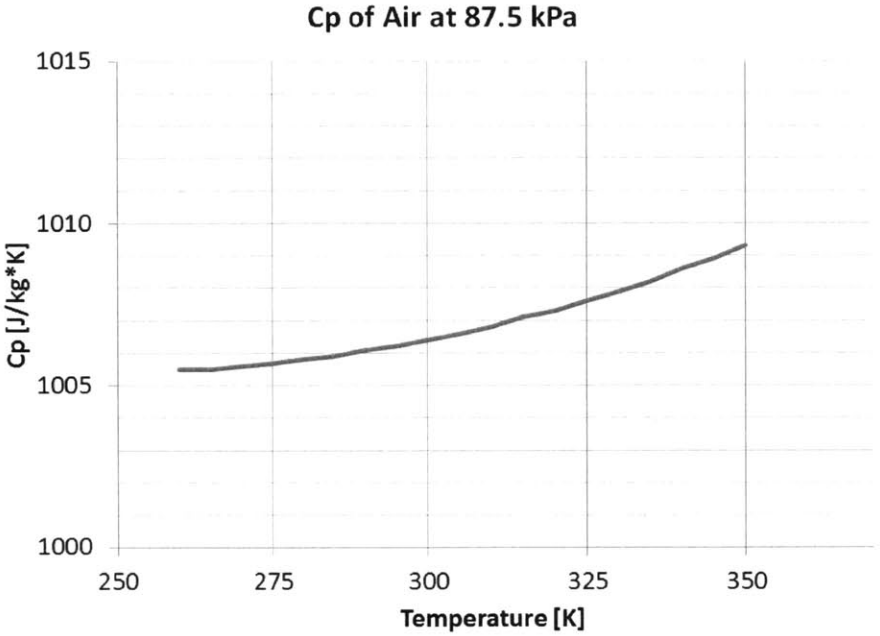

Figure 2-21: C_p of Air at 87.5 kPa

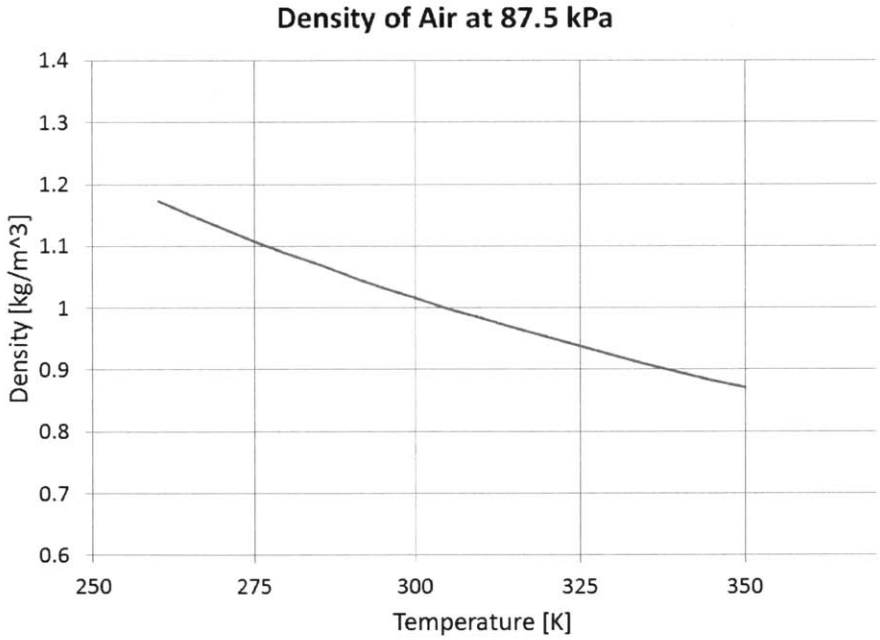

Figure 2-22: Density of Air at 87.5 kPa

2.5.3 Heat Exchanger Oil Model

The heat exchanger oil properties are utilized in the preliminary sizing calculations, the OCC simulation and the COMSOL simulation of the TES block. The models for the oil viscosity, thermal conductivity density and heat capacity are built into COMSOL. The oil is assumed to be incompressible and it's properties are assumed to be functions of temperature only.

2.5.4 Wholesale Electricity Prices

The primary purpose of this system is to perform extra cooling at night, when ambient temperatures and wholesale electricity prices are low, to allow for extra production during the day, when temperatures are high and wholesale electricity prices are high. Historical wholesale electricity prices are employed to help estimate the financial benefits of the system. Due to data availability, pricing information for the adjacent Midwest Region was used. [6]

This transient pricing data is used in conjunction with the predicted output of the plant to determine the estimated gross financial income for each time step. The income for standard plant is tracked along with that of the TES enhanced system to allow for a cost benefit analysis of the results.

Chapter 3

Results

3.1 System Dimensions and Cost

Table 3.1 shows the dimensions, configuration and cost of the modeled TES system. The system consists of 79 pipes of 0.66 m inner diameter. Each pipe is embedded in the concrete thermal storage block such that it is surrounded by a cylinder of concrete 1.155m in diameter. When the system is in operation 10,000 $\frac{kg}{s}$ of oil is circulated through all 79 pipes. This corresponds to a flow velocity of 0.423 $\frac{m}{s}$ and a Reynolds number of 23,250 (turbulent regime).

Approximately 70,500 metric tons of iron piping and 279,000 m^3 are required to build the thermal storage block. Based on assumed material costs of $400 per ton of iron pipe and $50 per cubic meter of concrete, this structure would cost approximately $45,000,000 in materials.

3.2 System Transient Performance

Figure 3-1 compares the net power generation of the standard 252 fan ACC operation to the TES enhanced 252 fan ACC plus 252 fan ACHX system. Ambient temperature fluctuations have a minor effect on the net power generation of the standard system. This is because the 252 fan ACC unit maintains the minimum condenser pressure of 300 kPa until ambient temperature is over 280K. The minor fluctuations in net

D_{hpipe}	0.66m
$D_{oconcrete}$	1.155m
thk_{pipe}	.011m
L_{pipe}	5000m
$Count_{pipe}$	79
v_{oil}	$0.423\frac{m}{s}$
Re_{target}	23250
m_{pipes}	70,500 metric tons
$V_{concrete}$	$279,000m^3$
MaterialCost	$\$45,000,000$

Table 3.1: System Dimensions and Cost

pressure that are present are due to changes in fan power due to fluctuations in ambient air density.

The TES enhanced operation is shown to have reduced power generation for times outside of the 11:00-20:00 window when oil cooled condensing (mode 3) is allowed. This is due to additional parasitic load of the ACHX fans and pumping requirements. During oil cooled condensing operation the net system power generation is slightly higher than the standard operation. During this time the condenser pressure is at it's minimum and the gross turbine power is at it's maximum for both standard and TES enhanced operation. However, the parasitic load of the ACC fans in standard operation exceed that of the oil pumping load in mode 3 operation.

Figure 3-2 shows the first week of June operation. The first and fifth days never enter mode 3 operation. The ambient temperature is low enough that ACC operation is preferred to OCC operation and the TES is apparently sufficiently cool to preclude ACHX cooling. Therefore, the system reverts to mode 1 operation and the TES enhanced power generation is identical to the standard operation.

The second, third and fourth days of June are good examples of operation during intermediate months. Mode 3 operation on the second day of June benefits from at least two nights worth of cooling, so its net power generation is higher than the subsequent nights. The third and fourth nights of June enter mode 3 operation with a TES block and oil that has only had the benefit of one night of cooling at warmer

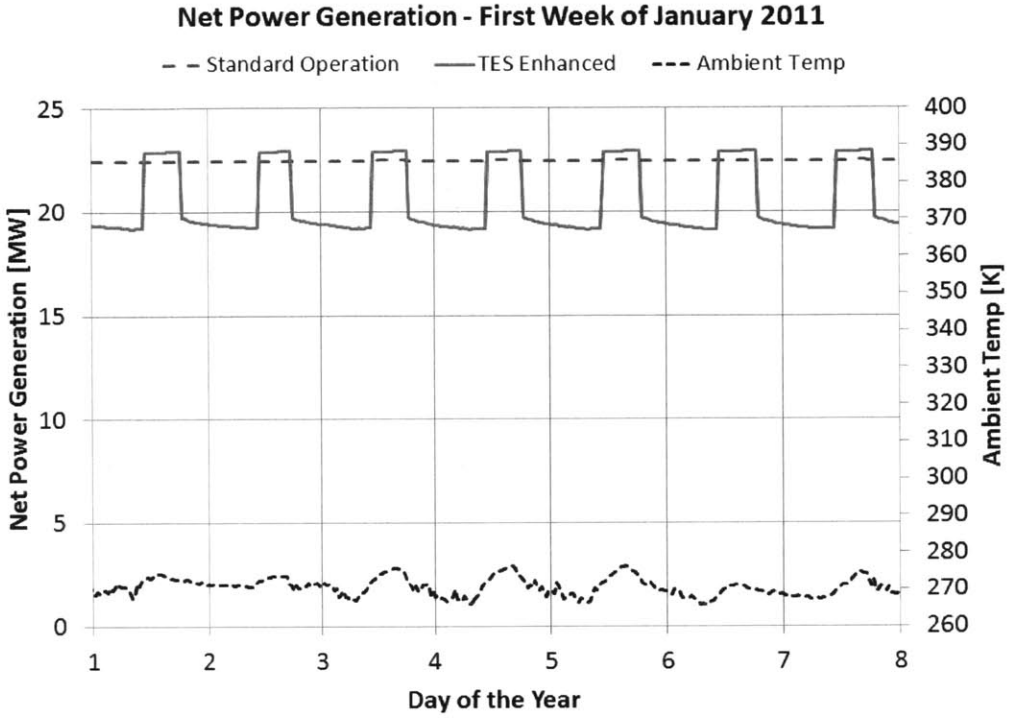

Figure 3-1: System Operation - First Week of January

ambient temperatures. Therefore, the peak mode 3 powers can be seen to drop off gradually.

By July the ambient temperature has warmed to the point that the system is almost exclusively in mode 2 and mode 3. See Figure 3-3. During mode 2 operation, the standard operation generally exceeds the output of the TES enhanced system by just over 2 MW. This is additional parasitic load from ACHX fans and oil pumping across the ACHX. The mode 3 power generation advantage varies depending on how fast the ambient temperature rises during the day, but it is generally between 2 and 7 MW during the warmer months.

3.3 TES vs Standard Operation Performance

Figures 3-4 and 3-5 compare the daily On-Peak and Off-Peak energy production levels for TES enhanced and standard operation strategies over the course of the year between November 8, 2010 and November 7, 2011. The Off-Peak production values

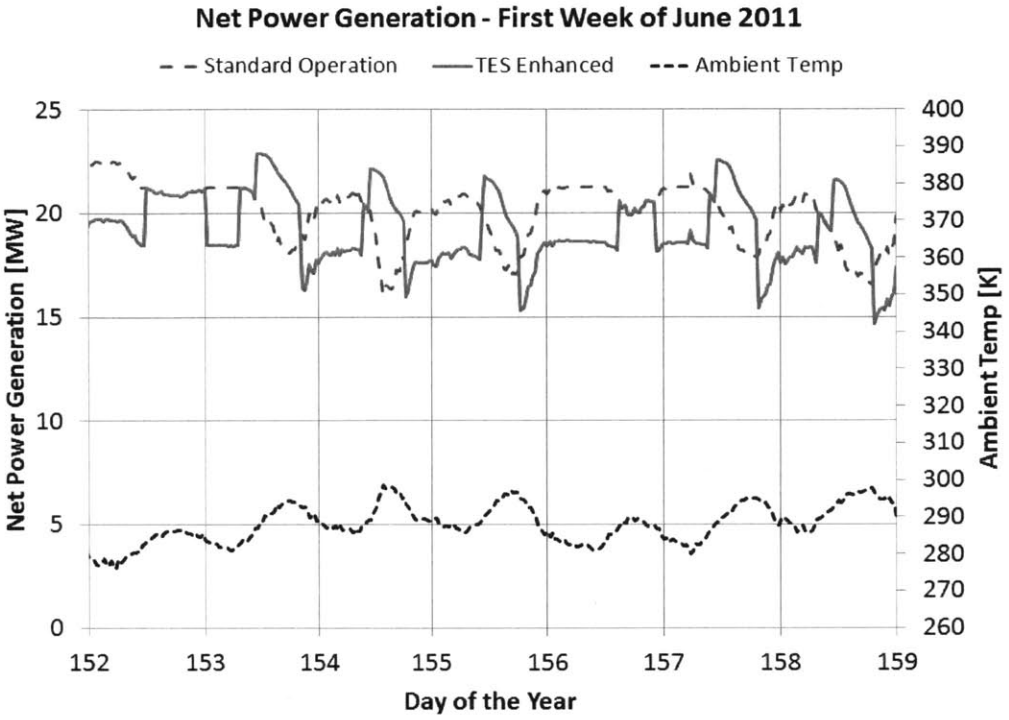

Figure 3-2: System Operation - First Week of June

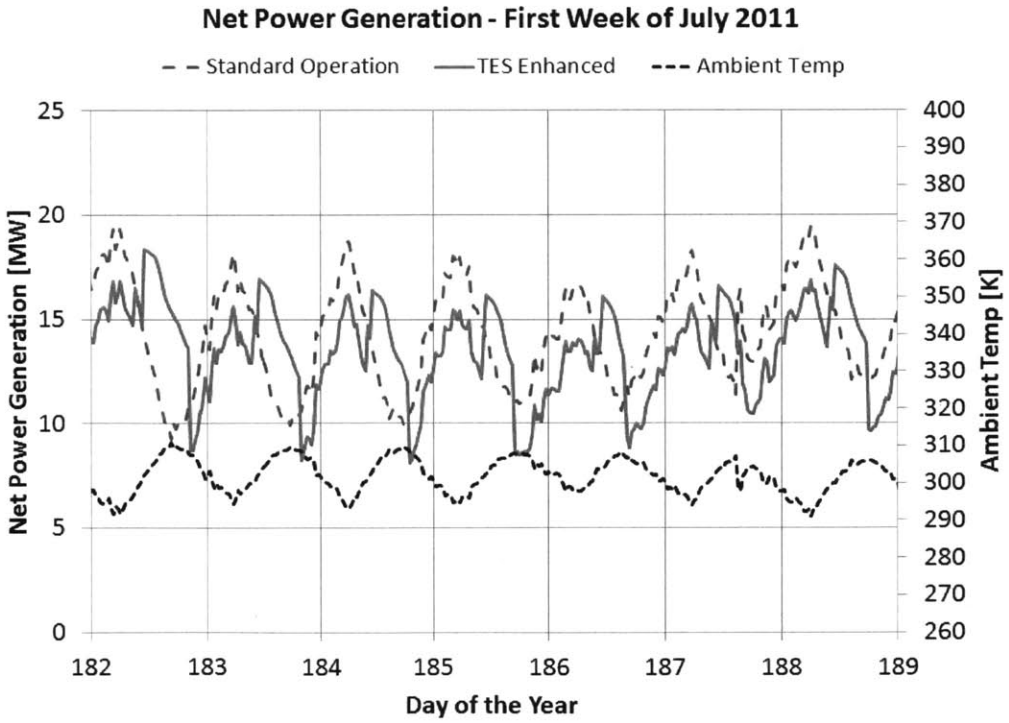

Figure 3-3: System Operation - First Week of July

are expected to be lower for the TES enhanced system. Running the TES support equipment such as the oil pumps creates additional parasitic load at some times and shifts some parasitic load, such as cooling with the ACHX from peak times to off peak times.

The trend in the On-Peak production is more complex. It is expected that the colder months favor standard operation and this trend is observed. During the warmer months, some days show a TES advantage and others do not. Another look at the first week of July 2011 begins to clarify the situation. Examination of Figure 3-6 suggests that the relationship between the maximum temperature of a given day and the minimum temperature of the previous night may determine the TES advantage over standard operation. That is, a hotter day followed by a cooler night seems to result in greater TES advantage.

Figure 3-7 reinforces this hypothesis as it shows a positive correlation between the TES enhanced on-peak production advantage and the temperature excursion between the previous night and a given day. The figure shows only the warmest months, but the positive correlation is present for the whole data set. The scatter is significantly greater for the cold months however. If this system is to be constructed and implemented, the control system must leverage this correlation between weather conditions and the performance advantage of operating the TES system.

3.4 Economic Assesment

Shifting energy production from off-peak to on-peak hours is important for matching production to grid demands. However, understanding the profitability of this technology is critical to assessing whether it will actually be implemented. The capital costs of the proposed system are in the tens of millions of dollars and the payback period is an important consideration when utilities are assessing investments.

The daily income advantage of the TES enhanced system is related to the daily on peak energy production advantage. However, price fluctuations throughout the day can affect the relationship based on whether high prices occur during mode 3

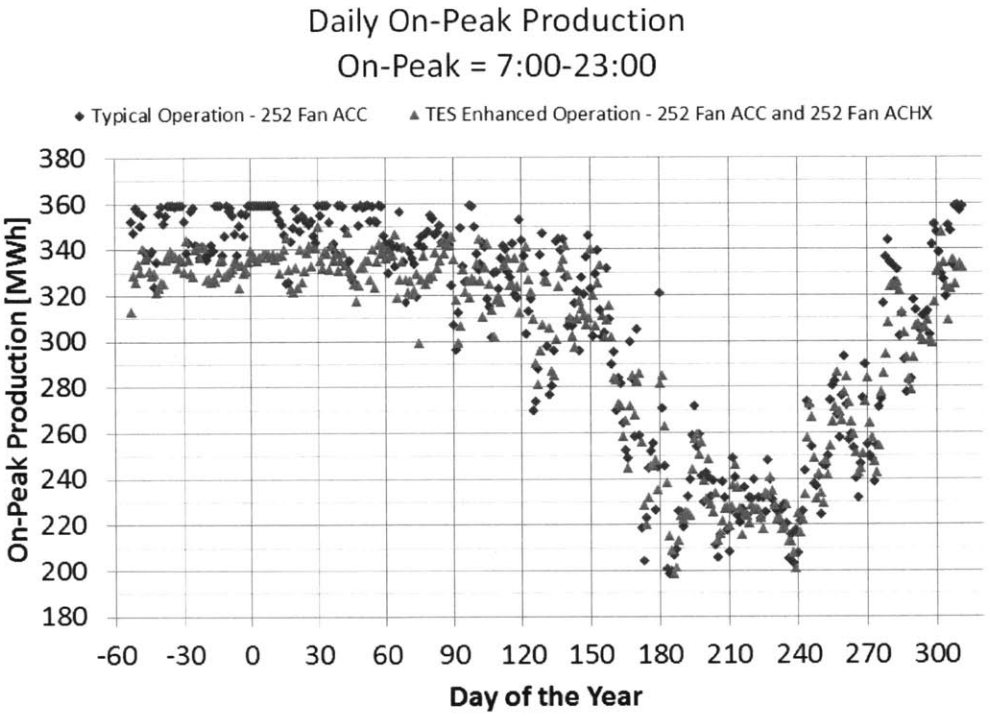

Figure 3-4: Daily On Peak Production

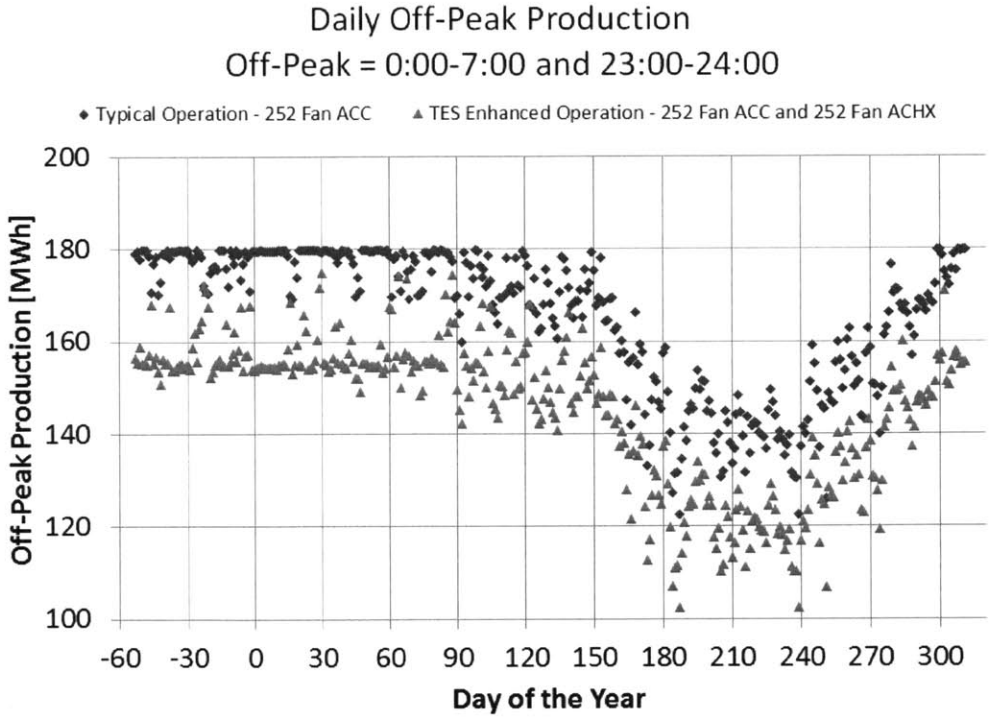

Figure 3-5: Daily Off Peak Production

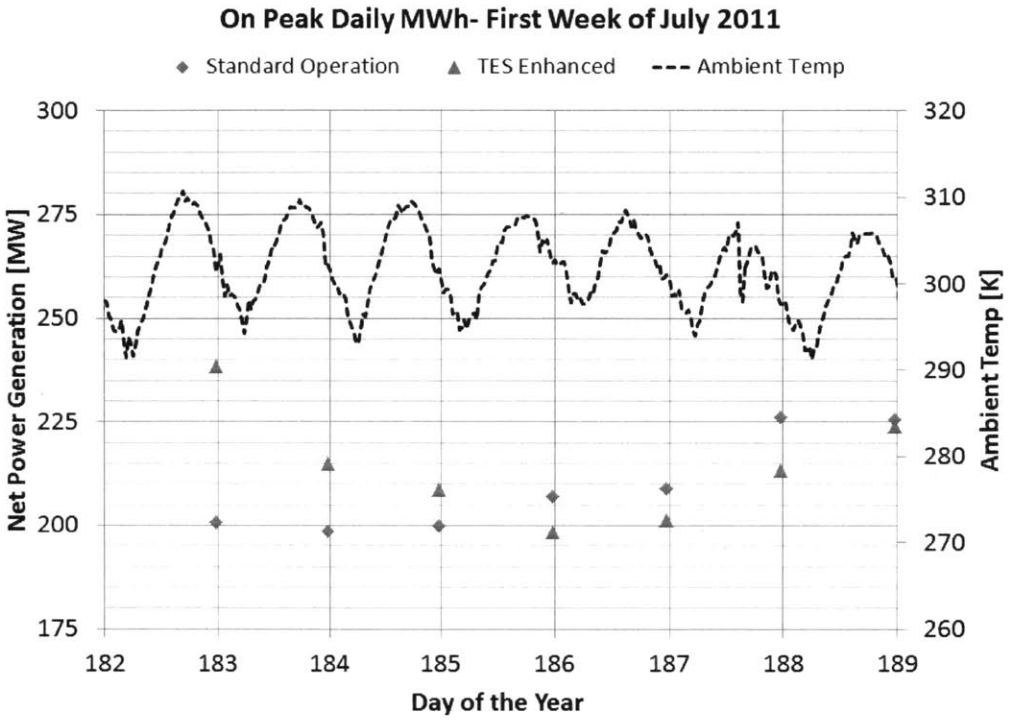

Figure 3-6: Daily On Peak Comparison - First Week of July 2011

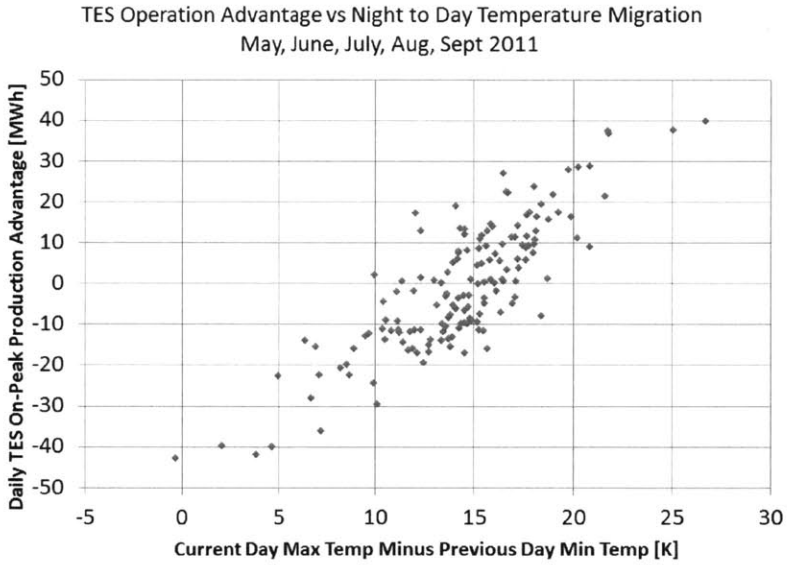

Figure 3-7: TES On-Peak Advantage vs Night to Day Temperature Swing

operation when TES enhanced production is higher than standard production or during mode 2 operation when TES enhanced production is a handicap in relation to standard ACC-only production.

Figures 3-8 and 3-9 show the standard and TES enhanced power generation along with the Midwest U.S. wholesale electricity price for the first week of January and July respectively. Most days have distinct price peaks during the day. Periods of elevated wholesale prices often occur during the 11:00-20:00 time period when mode 3 operation is allowed. However, some days have peak price times that fall outside of the mode 3 operation window. This can lead to an income distandard 252 fan ACC advantage, even when the system is performing as intended.

Figure 3-10 depicts the ratio of the daily TES enhanced income to that of standard operation. Figure 3-11 shows the correlation between daily income advantage as a function of the daily energy production advantage. This demonstrates that the unpredictable nature of wholesale electricity prices can negatively effect the income generated even on a day when more electricity is generated under TES enhanced operation. This is significant, as it is likely easier to predict near term weather trends than electricity prices.

A sum of the daily income exclusively for days of positive energy production advantage is used to estimate the financial benefits possible in a TES enhanced system under weather forecast enabled control. Figure 3-12 compares this estimation of the potential income advantage to the cumulative income difference of the system as run. This shows an estimated annual income advantage of $25,000. This is insufficient to justify the estimated $45,000,000 in material costs necessary to construct the proposed cold side TES system.

In order to estimate the economic cost of the parasitic loads associated with the TES system, the energy required to run the oil pumps and ACHX are completely neglected. In this case, the annual economic advantage of the TES enhanced system is $189,000 as compared to $25,000 per year with the calculated parasitic loads. Even under such optimistic assumptions the income advantage of the TES enhanced system does not justify the required capital cost.

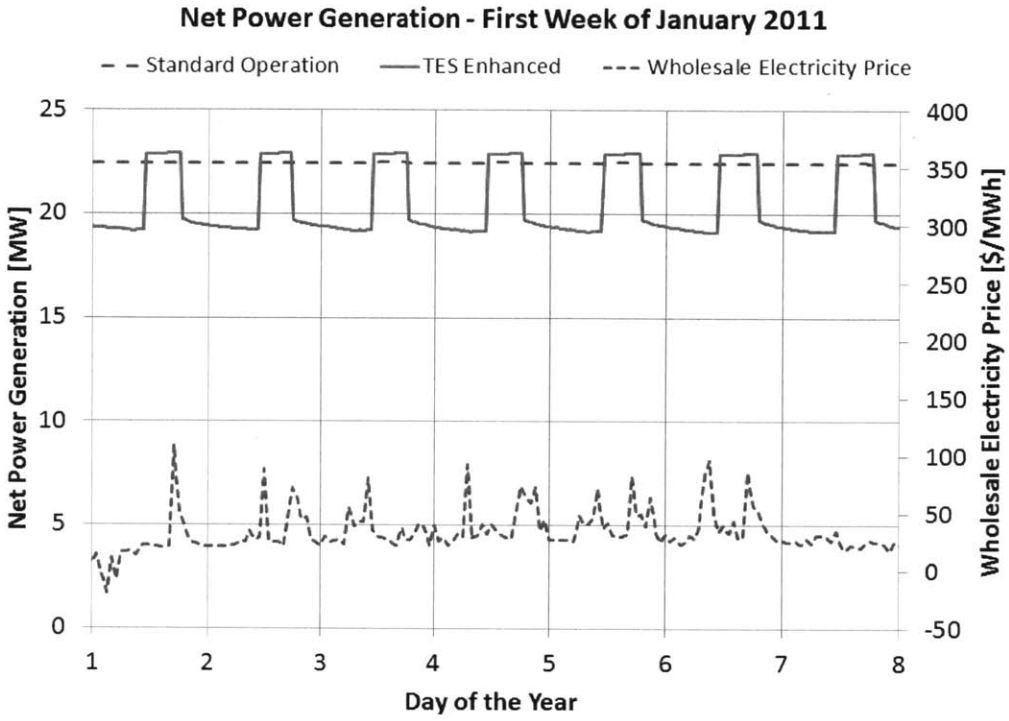

Figure 3-8: Net Power Comparison With Wholesale Prices - January 2011

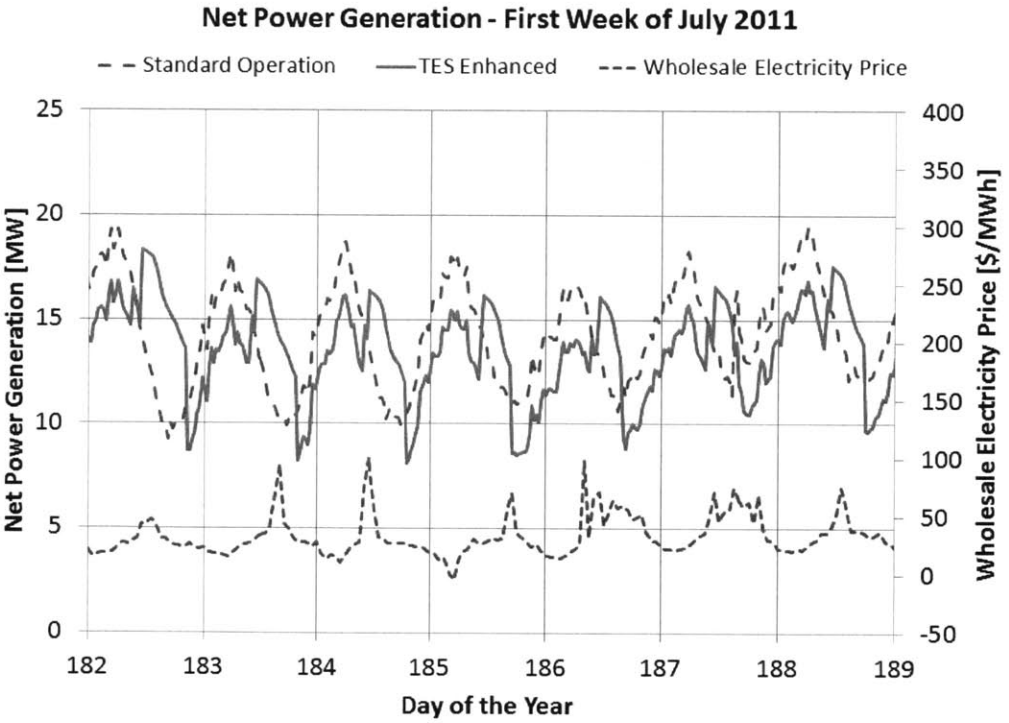

Figure 3-9: Net Power Comparison With Wholesale Prices - July 2011

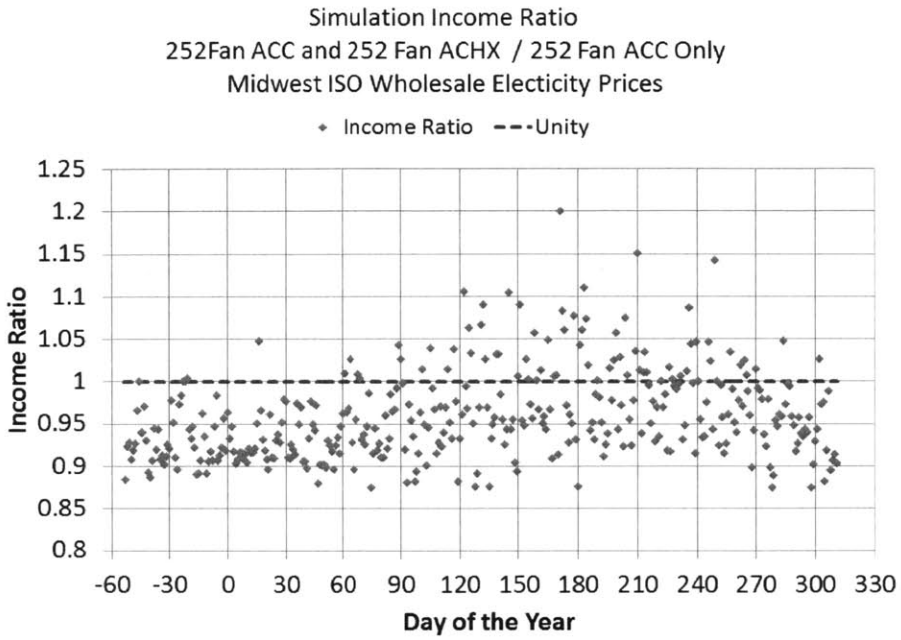

Figure 3-10: Simulation Daily Income Ratio

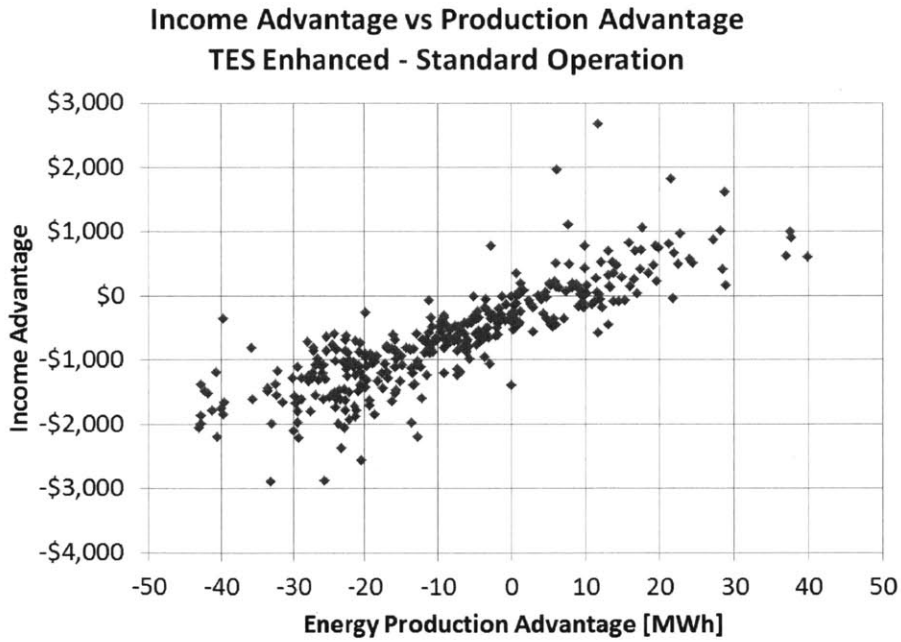

Figure 3-11: Income Advantage vs Production Advantage

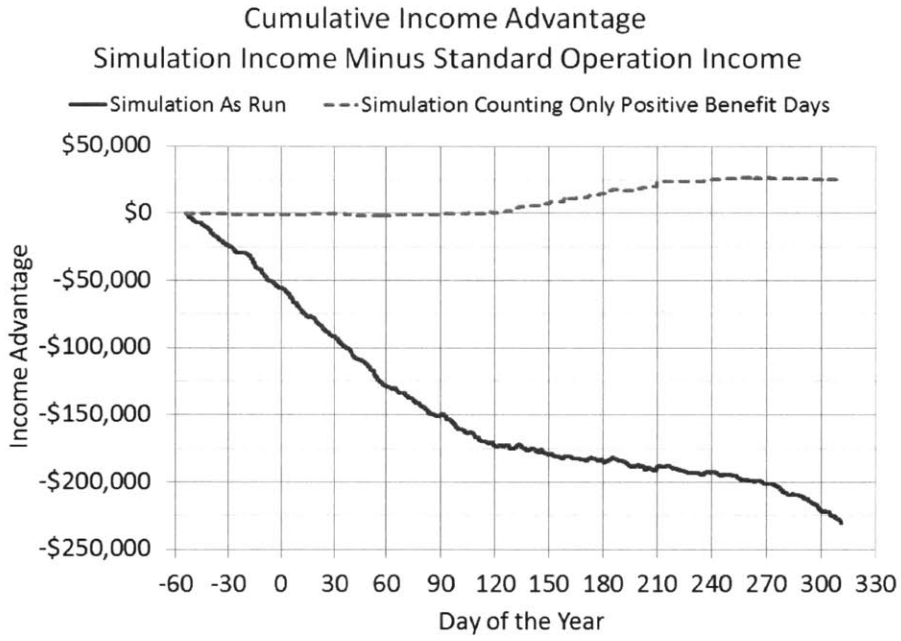

Figure 3-12: Income Advantage: Positive Benefit Days vs As Run

Chapter 4

Discussion

4.1 System Value

This analysis demonstrates that a cold side thermal energy storage system is capable of effectively shifting production capacity of a dry air cooled power plant from night time to day time. However, the additional equipment required to facilitate the thermal energy storage lead to increased parasitic loads. The potential value of these parasitics loads is variable in the context of predicted future weather patterns. Therefore, a well designed control system capable of leveraging weather predictions and monitoring TES block thermal potential is necessary to maximize plant energy production.

Even with such a control system the simulated TES enhanced plant does not always generate more energy in a given day than the standard operation. The increased parasitic loads to facilitate the multi-mode operation reduce the effective advantage of the thermal storage system to the point where changes in ambient temperature patterns can determine which mode is most productive.

The unpredictable nature of wholesale electricity prices introduces an additional challenge to profitability of a TES enhanced system. While an increase in on-peak production is generally correlated with an increase in daily income, this correlation is subject to some uncertainty based on market conditions. This is largely due to the fact that increased production at one time of day must be coupled with decreased production at a different time of day. These fluctuations must coincide with beneficial

fluctuations in electricity price in order to ensure a positive income advantage.

In spite of sensitivity to market conditions, it is shown that a positive income advantage for the TES system is possible assuming an appropriate control system is employed. However, the magnitude of this income advantage is unlikely to result in an acceptable payback period to recover the capital investment to actually build the system.

4.2 System Shortcomings

4.2.1 Small Usable Temperature Range

The main disadvantage of the cold side TES concept is the relatively small temperature range over which the thermal storage medium operates. In the case described, the temperature migration of the storage medium is limited approximately to the daily migration in ambient temperature. It is impossible to drive its temperature even as low as the nightly minimum temperature and the oil cooled condensing strategy loses it's advantage over air cooled condensing as the medium temperature exceeds the daily max by more than a few degrees.

The required mass of the thermal medium is inversely proportional to the usable temperature range over which it is to be employed. Larger temperature operating ranges results in a smaller system size relative to the energy storage capacity. Usable heat transfer levels are also easier to attain in the heat exchange equipment when greater temperature differences are present. The capital costs of building the system and parasitic losses associated with pumping heat exchange fluid through the TES are therefore both likely to be reduced for systems designed to operate over greater temperature ranges.

This suggests that TES systems are likely more easily applied to hot side applications such as storing thermal energy from a concentrated solar power facility for use after sunset. Such a hot side TES system could store thermal energy at a greater density than a cold side TES if the associated power cycle is designed to operate over

a sufficiently large range of heat source temperatures.

4.2.2 Dependence on Traditional Air Cooled Heat Exchangers

The other key shortcoming of the proposed cold side TES system is the dependence on traditional air cooled heat exchange units. These units require too much power to drive relatively high velocity air over the finned coil bundles. This power penalty during the TES cooling phase limits the profitability of the overall system.

The proposed system is configured to use air cooled heat exchange that is not optimized for the working fluid and flow rates required of it. Therefore, it may be over-penalized for certain types of losses such as the pumping power required to drive the heat exchange oil across the ACHX. A custom designed unit may be able to reduce this loss. However, even significant reductions in the required pumping power fail to change the capital payback period to that of a realistic investment.

4.3 Future Research

If cold side systems are to be pursued, then alternative cooling systems should certainly be investigated. Reduced reliance on high powered fans reduces the parasitic load induced during cooling periods. Successful reduction of this parasitic load allows for the same periods of increased daytime output without the significant penalty during cooling. If sufficient reductions on parasitic loads are achieved, the predicted annual economic advantage of the system comes closer to justifying the capital expenditures necessary to construct it.

A low parasitic system should take advantage of the large dimensions of the TES block to provide large heat exchange areas. For example, an actuated ventilation system on an insulated enclosure could facilitate a range of cooling schemes from low velocity fan driven cross flow to chimney enhanced natural convection using cool night time air. Spreading the heat exchange over such an enormous area allows for

large heat flux without the necessity for high potential concentrated in fan driven cooling units. One time construction costs of such a system would exceed those of a simpler insulated block, but the reduction in parasitic load may provide meaningful improvements in system profitability.

If such advanced cooling concepts are found to be impractical, the proposed system offers opportunity for several specific improvements. First, the air cooled heat exchange units must be designed for the higher flow rate and different material properties of heat exchange oil as opposed to the isobutane that they are intended for. Significant reductions in pumping power are likely a valuable stepping stone towards reducing the parasitic loads incurred by this system.

The control system offers another opportunity for improvement. Integration of a weather prediction methodology with the dynamics of the TES block and cooling apparatus could lead to meaningful output improvements. Careful integration of a real time electricity price monitoring program could also lead to efficiencies for the TES cooling control. For example the equations to assess the value of running the ACHX should be modified to leverage knowledge of current prices. This logic is particularly profitable in cases of negative prices when ACHX fans will gladly make good use of excess electricity.

Bibliography

[1] COMSOL AB. Comsol 4.2a. Software, 2011.

[2] alibaba.com. Supply hot cast iron pipe with best price. `http://www.alibaba.com/productgs/430304650/supply_hot_cast_iron_pipe_with.html`. Accessed April 2012.

[3] Y. Cengal and R. Turner. *Fundamentals of Thermal-Fluid Sciences.* McGraw Hill, New York, USA, 2001.

[4] R. DiPippo. *Geothermal Power Plants.* Butterworth-Heinemann (Elsevier), Boston, MA, second edition, 2008.

[5] H. Ghasemi, A. Tizzanini, M. Paci, and A. Mitsos. Modeling and optimization of a binar geothermal plant. *Submitted: Energy*, July 30, 2012.

[6] Midwest Independent Transmission System Operator Inc. `https://www.midwestiso.org/Library/MarketReports/Pages/MarketReports.aspx`, 2010-2011. Midwest ISO Market Reports Site.

[7] Enrique Lizarraga-Garcia. Optimal operation and design of solar-thermal energy storage systems. Master's thesis, Massachusetts Institute of Technology, Cambridge, MA, 2012.

[8] NIST.gov. *RefProp.* 2007. Database 23 Version 8.0.

[9] B. Posner. Introduction to energy and earth sciences economics: Lesson 12 - topical issues: Changes in the electricity business. Lec-

ture, John A. Dutton e-Education Institute Pennsylvania State University, 2012. https://www.e-education.psu.edu/ebf200up/node/151, This figure is reproduced under the Creative Commons License (available at https://creativecommons.org/licenses/by-nc-sa/3.0/).